Bulletin of Engineering Geology and the Environment (2025) 84:609
https://doi.org/10.1007/s10064-025-04623-2

ORIGINAL PAPER

Einstein-Telescope in the Euregio-Meuse-Rhine – Preliminary engineering geological site characterization for siting and design

Raphael Burchartz[1,2] · Marius Waldvogel[2] · Nils Chudalla[3] · Peter Achtziger-Zupančič[4] · Helmut Wannenmacher[5] · Bjorn Vink[6] · Frank Linde[6] · Philippe Orban[7] · Yvonne Spychala[2] · Pooya Hamdi[1] · Mohammadreza Jalali[1] · Frédéric Nguyen[7] · Raul Fuentes[8] · Nastassja Berg[8] · Shahar Shani-Kadmiel[9] · Florian Wellmann[3,4] · Peter Kukla[2] · Florian Amann[1,4]

Received: 4 June 2024 / Accepted: 3 October 2025

Abstract
Modern gravitational-waves astronomy is moving underground. Geological units act as noise-dampening covers to isolate highly sensitive gravitational-wave detectors from ambient noise disturbances, which poses challenges for the siting, planning, and construction of detectors. The current feasibility study for the Einstein Telescope (ET), the European third-generation gravitational-waves detector, aims to find the most suitable site for construction and operation from various perspectives. One potential site is the Euregio-Meuse-Rhine (EMR) area in the border region between the Netherlands, Belgium, and Germany. The Einstein Telescope is planned as a large-scale underground infrastructure with over 30 km of tunnels and various cavern constructions, approximately 250 m below the surface. This paper presents the preliminary results of the first site characterization phase for this site from an engineering geological perspective. The results show (1) complex geological conditions of siliciclastic and carbonate, brittle and hard Paleozoic (Frasnian to Westphalian) rocks beneath a cover of soft, partly unconsolidated Cretaceous and Cenozoic sediments, (2) the strong influence of several tectonic events, especially the thrust-and-fault belt of the Variscan Front and the opening of the Lower Rhine Graben, (3) variable and in places high hydraulic conductivities (10^{-5} m/s) and, (4) variable rock mechanical properties of potential host rock formations (e.g. Famennian and Namurian rocks). Finally, an engineering geological assessment of the suitability, challenges, and requirements for future work associated with the construction of the ET in the EMR region is presented.

Keywords Einstein Telescope · Site selection · Euregio-Meuse-Rhine · Regional geology · Gravitational waves · Tunneling

✉ Raphael Burchartz
burchartz@lih.rwth-aachen.de

1 Chair of Engineering Geology and Hydrogeology, RWTH Aachen, 52064 Aachen, Germany

2 Geological Institute, RWTH Aachen, Aachen 52062, Germany

3 Chair of Computational Geoscience and Reservoir Engineering, RWTH Aachen, Aachen 52074, Germany

4 Fraunhofer Research Institution for Energy Infrastructures and Geothermal Systems IEG, Aachen 52062, Germany

5 Implenia Austria GmbH, Salzburg, Austria

6 Nikhef, Science Park 105, Amsterdam 1098 XG , The Netherlands

7 Urban and Environmental Engineering, University of Liège, Liège 1 4000, Belgium

8 Chair of Geotechnical Engineering and Institute of Geomechanics and Underground Technology, RWTH Aachen, Aachen 52074, Germany

9 Royal Netherlands Meteorological Institute (KNMI), De Bilt, Netherlands

Published online: 19 November 2025

Introduction

The Einstein Telescope (ET) is a planned third-generation gravitational-waves (GW) detector currently in the feasibility study stage. The structure will follow the Japanese Kamioka Gravitational Wave Antenna (KAGRA) as the next large-scale underground facility for the detection and investigation of small space-time strain originating from gravitational-waves (Somiya 2012; Fiori et al. 2021), and demands a minimum surface cover of approximately 250 m to minimize the disturbing effect of ambient environmental noise.

The currently favored design consists of a triangular interferometer geometry hosted in a tunnel and cavern system, with side lengths of approximately 10 km (Fig. 1) (Freise et al. 2009, 2011; Ronchini et al. 2022; Branchesi et al. 2023). The facility will host two different types of interferometers: a low-power, low-frequency cryogenic detector and a high-power, high-frequency room temperature detector (Amann et al. 2020; Di Pace et al. 2022; Ronchini et al. 2022). This layout is expected to improve detector sensitivities by one order of magnitude to frequencies as low as 1 Hz (Punturo et al. 2010; Hild et al. 2011; Sathyaprakash et al. 2012; Beker et al. 2015; Di Pace et al. 2022).

However, the sensitivity and operational efficiency of gravitational-wave detectors are significantly influenced by ambient noise, such as thermal, seismic, and Newtonian noise, which necessitates a quiet, well-isolated underground environment to maximize the performance and reliability of measurements (Hild et al. 2011; Amann et al. 2020; Koley et al. 2022). Consequently, siting is dominated by the demand for low ambient seismic noise, particularly in the frequency band between 1 and 10 Hz, as well as favorable geological conditions for excavation processes and noise attenuation characteristics.

Soft geological units have demonstrated a proven capability as attenuators for ambient seismic and subsequent Newtonian noise, potentially lowering seismic-wave propagation by several orders of magnitude (Akutsu et al. 2018; Koley et al. 2022; Di Pace et al. 2022). However, realizing a large-scale underground infrastructure introduces additional engineering demands. Site selection must satisfy a complex set of criteria encompassing geological, technical, financial, and socio-political considerations (Amann et al. 2020). Geological and engineering-geological factors, such as rock mass strength, in-situ stress conditions, fracture networks, and hydrogeological parameters like hydraulic conductivity and storativity, are critical for selecting suitable excavation methods, drainage, and support design. These factors are particularly important at the corner points, where large caverns and access structures (e.g., ramps, shafts) will be constructed. Hydraulic rock mass properties have a significant influence on groundwater inflow during both construction and operation, necessitating proactive measures such as grouting and pumping strategies to mitigate this impact. These processes can introduce additional noise and must also account for potential surface subsidence (Amann et al. 2020).

Following an investigation of different candidate sites for the ET over recent years, two sites were chosen for more detailed study (Amann et al. 2020): the former Sos-Enattos mining region in Sardinia, Italy, and the Euregio Meuse-Rhine (EMR) in the three-border region of Belgium, Germany, and the Netherlands. Intensive efforts have since been devoted to assessing the suitability of both potential regions for constructing and operating the Einstein Telescope (Di Pace et al. 2022). Recently, a third site in Lusatia (eastern

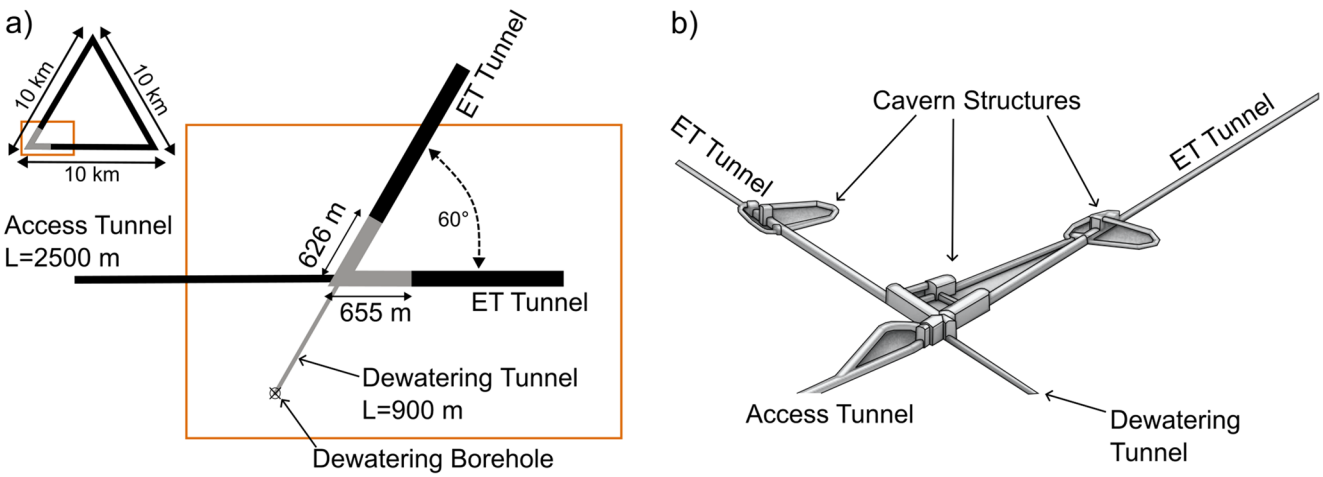

Fig. 1 (**a**) Schematic impression of potential ET corner point with indication of cavern system (grey) and tunnel types. The stated dimensions can vary. (**b**) Potential cavern and tunnel complex at ET corner point. Not to scale. The example shows the access via an inclined access tunnel (modified after: Implenia Austria GmbH, unpublished)

Germany) has also been designated as an official ET candidate site.

This contribution explicitly addresses the preliminary geological and geotechnical assessment of the EMR candidate site from an engineering geological perspective. It forms part of the Einstein Telescope Euregio-Meuse-Rhine Site & Technology (E-TEST) project, which aims to establish the preliminary feasibility of subsurface conditions in this region. A central aspect of the investigation is identifying a suitable site perimeter within the EMR through a stepwise exclusion approach. This involves filtering based on (a) ambient seismic noise sources such as wind-turbines, traffic, and railway, (b) geological constraints such as fault zones, and (c) environmental sensitivities like nature reserves.

While ambient noise characterization is an essential aspect of the overall site selection, the focus of this work is on the geological and geotechnical suitability of the subsurface environment. This includes rock strength, in-situ stress conditions, fracture networks, and hydrogeological parameters, all of which are fundamental to ensuring the safe and cost-effective construction of the planned underground infrastructure. The geological and engineering geological investigations presented here serve as a foundation for estimating excavation strategies, evaluating rock mass behavior, and assessing construction feasibility.

The data collected provides critical input for the forthcoming 3D geological model of the region and will support the optimal siting, layout, and design of the Einstein Telescope, thereby contributing to the project's long-term operational success.

The EMR site at a glance

The Euregio Meuse-Rhine (EMR) is the three-border region between Belgium (BE), the Netherlands (NL), and Germany (GER). It covers the provinces of Limburg (in both Belgium and the Netherlands), Liège, and the Aachen region. Despite its proximity to larger cities such as Liège, Maastricht, and Aachen, the Belgian-Dutch-German border region is predominantly agricultural (Koley et al. 2019). The potential site for the Einstein Telescope within the EMR, as investigated in this study, spans approximately 1,000 km^2 and includes parts of Wallonia, Flanders, Dutch South Limburg, and the Aachen region.

Centered in the heart of the EMR, the site is characterized by the hilly landscape of the Venn Foreland and the Loess area of southern Limburg (Mönnig 2007). To the South, it abuts elevated plateaux of the Eifel and Ardennes mid-mountain ranges.

Geologically, the study area is highly heterogeneous, comprising sedimentary and metasedimentary formations from the Cambrian to the Quaternary. Notably, stratigraphic discontinuities are present between the Lower Ordovician and Lower Devonian, as well as between the Upper Carboniferous (Westphalian) and the Upper Cretaceous. An overview of the surface geology is provided in Fig. 2, while the major lithostratigraphic and tectonic phases are summarized in Fig. 3.

The oldest rock units, of Upper Cambrian to Lower Ordovician (Tremadocian) age, are exposed in the southeastern corner of the study area and form part of the Brabant massif in the subsurface west of the study area (TNO 2004; Walter 2007). These units predominantly consist of alternating quartzite-black shale and sandstone-phyllite sequences (Laloux et al. 2000). Due to intense thrust faulting associated with Variscan compression, estimates of thickness are uncertain, however, total thicknesses are believed to exceed 1,300 m (Laloux et al. 2000).

Within the E-TEST study area, these strata form the older Paleozoic basement, which is discordantly overlain by younger Paleozoic sedimentary units ranging from the Lower Devonian to the Upper Carboniferous (Westphalian). Among these, parts of the Upper Devonian (Famennian) continental to shallow marine sandstone and siltstone complex, known as the Condroz Sandstone Group (Laloux et al. 2000; Thorez et al. 2006; Walter 2010), represent promising host rock conditions for caverns at the ET vertices. They are therefore of high interest in the siting process. This group shows local thickness of up to 400 m. The lower 100 to 150 m mainly consist of thinly bedded, mica-rich, arcosic sandstones, frequently alternating with shale and siltstone beds (Esneux Member) (Walter 2010; Mottequin et al. 2024). They are overlain by a succession of up to 250 m thickness, beginning with arkosic and quarzitic, massive sandstones (Monfort Member), followed by a transition into a heterolithic sequence comprising shale, siltstone, and arkosic, locally highly micaceous sandstones (Evieux Member) (Walter 2010; Mottequin et al. 2024). In the uppermost Condroz Sandstone Group, a progressive increase in carbonate cementation and first intercalations of dolomitic limestone indicate the transition to a shallow marine depositional environment (Laloux et al. 2000; TNO 2004; Walter 2010).

The Lower Carboniferous is present as thick (up to >400 m) successions of carbonate rocks, firstly dolomitic in Tournaisian units with a transition to limestones of Viséan age, deposited in a shallow marine setting (Bless et al. 1980, 1983; Hance et al. 1999; TNO 2004; Walter 2007, 2010; Poty 2016). The contact between the uppermost Lower Carboniferous limestones and the Upper Carboniferous (Namurian) may exhibit bedding-parallel paleokarst features, resulting from subaerial exposure during the Variscan orogeny (Laloux et al. 2000).

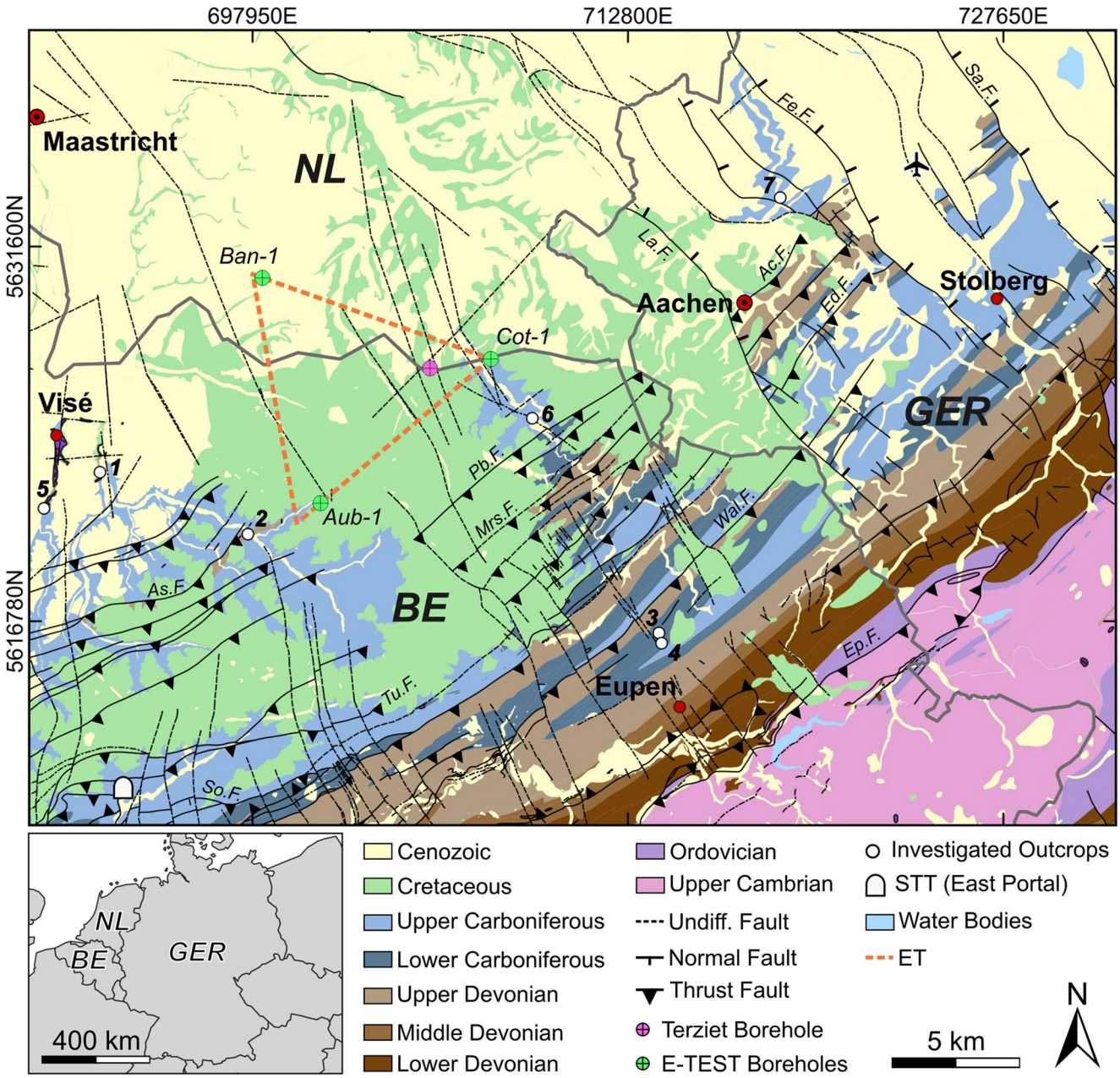

Fig. 2 Simplified geological map of the investigation area showing the surface distribution of stratigraphic units and major fault structures. Key elements of the E-TEST project are indicated, including E-TEST boreholes (green circles), prior boreholes (pink circles), and investigated outcrops (numbered white circles). The proposed layout of the Einstein Telescope (ET) is outlined in orange, and the location of the Soumagne Train Tunnel (STT) east portal is marked. Please note that the geological units shown represent the surface geology and do not reflect subsurface conditions at the projected tunnel depth. These conditions will be further characterized through ongoing investigations and integrated into a forthcoming 3D geological model. The proposed ET layout used in this study is preliminary and does not necessarily reflect the final configuration. Fault zone abbreviations: As.F. = Asse Fault, Tu.F. = Tunnel Fault, Ep.F. = Eupen Fault, Wal.F. = Walhorn Fault, Mrs.F. = Morsenet Fault, Pb.F. = Plombières Fault, La.F. = Laurensberger Fault, Ac.F. = Aachen Fault, Ed.F. = Eilendorf Fault, Fb.F. = Feldbiss Fault

Namurian deposits start as fine-grained shale and siltstone successions with notable mica content. They gradually change to coarser-grained silt- and sand-stones, indicating a transition from a marine to a coastal or terrestrial environment (Bless et al. 1980, 1983; TNO 2004; Walter 2007, 2010). This unit is characterized by thick (several metres), bedded (quartzitic) sandstones that are interbedded with thin (few centimetres) conglomerate layers (Laloux et al. 2000). These successions are overlain by marine black shales with a thickness of several tens of metres, followed by alterations

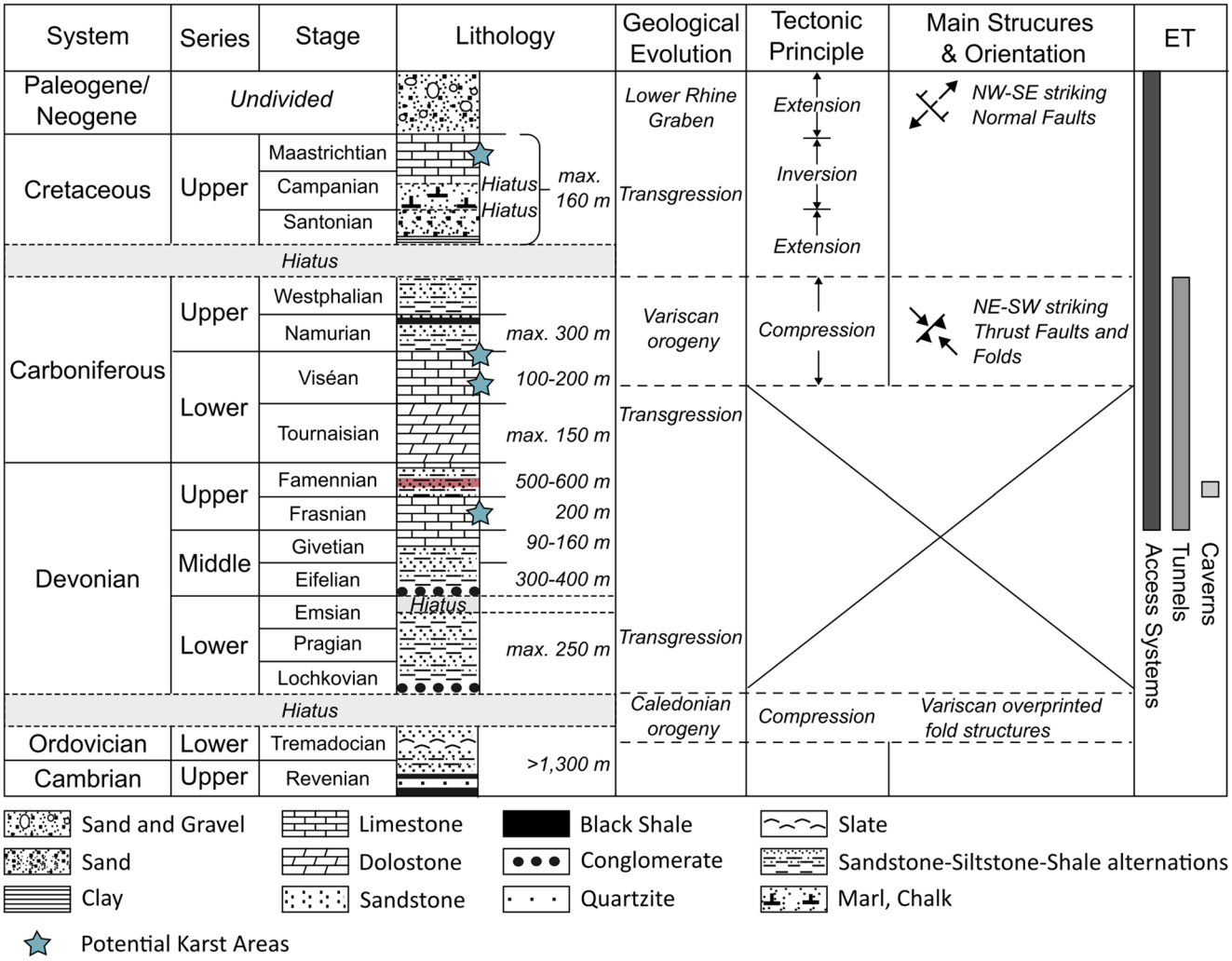

Fig. 3 Lithostratigraphic and structural overview of the study area, showing the main geological units, principal tectonic phases, and dominant structural orientations. The figure also indicates which stratigraphic intervals would be intersected or impacted by the planned Einstein Telescope (ET) infrastructure, including the main caverns, tunnels, and access systems. The Condroz Sandstone Group is indicated as red band in the lithostratigraphic column. The Lithostratigraphic column and thickness estimates are based on Laloux et al. (2000) and Walter (2010)

of sandstone and siltstone (Laloux et al. 2000). In Belgian parts of the study area, the Namurian successions show a maximum thickness of 300 m.

Rock units of Westphalian age show a limited appearance on the surface of the study area (limited to a few outcrops mainly within the Wurm valley, Germany). Still, they are described as remnants of past coal mining activities in the Aachen area and southern Limburg (Netherlands). They mainly consist of sandstone, siltstone, and shale successions of variable thickness, intersected by coal seams (Walter 2010). Thickness estimates are challenging due to the absence of outcrops.

Between the Upper Carboniferous to the Upper Cretaceous, the region experienced a prolonged period of non-deposition. From the Upper Cretaceous onward, shallow marine sediments, comprising chalk, sands, silts, clays, marls, and Cenozoic marine and fluvial sediments, as well as aeolian loess were deposited unconformably on the Paleozoic basement (Walter 2010). The Upper Cretaceous succession, ranging from Santonian to Maastrichtian in age, begins with sandy, silty, and clay-rich deposits of the Aachen Formation (Santonian), which are unconformably overlain by calcareous to marly sands of the Vaals Formation (Lower Campanian). From the Upper Campanian onward, the succession is dominated by calcareous units of the Gulpen Formation (Upper Campanian to Upper Maastrichtian) and the Maastricht Formation (Upper Maastrichtian), composed primarily of marls, chalk, and limestone (Bless et al. 1986; Laloux et al. 2000). In the study area, these mostly unconsolidated sediments might reach local thicknesses of up to 160 m and pinch out towards the south.

During the Carboniferous the Paleozoic basement underwent strong folding and faulting due to compression tectonics, which resulted in the creation of the fold-and-thrust belt of the Variscan Front Zone (Cambier and Dejonghe 2010). Consequently, numerous thrust faults with a prominent SW-NE strike strongly superimposed the Paleozoic rock units. Major thrust faults in the study area (i.e., Morsenet-, Tunnel-, Asse-, Aachen-, and Walhorn-Fault) exhibit a dip-slip component of several hundred metres to kilometres (Cambier and Dejonghe 2010, 2012). Subvertical, NW–SE striking normal faults (i.e., the Felbiss-Fault and the Laurensberg Fault), which have been repeatedly reactivated since the Variscan orogeny, intersect the Variscan thrust faults nearly orthogonally (Deckers et al. 2023). These structures are now part of the Lower Rhine Graben, which is associated with the European Cenozoic Rift System (Geluk et al. 1994; Camelbeeck et al. 2007; Deckers et al. 2023), and affect geological units ranging from Paleozoic to recent.

Comprehensive structural geological studies of the area have been conducted by Camelbeeck et al. (2007), Geluk et al. (1994), Hollmann (1997), Houtgast and van Balen (2000), Poty and Delculée (2011), Trautwein-Bruns et al. (2010, 2011), and von Winterfeld (1994). A systematic fault zone inventory of Belgium, including the Northeastern Wallonian region, has been compiled by Cambier and Dejonghe (2010, 2012).

The strong tectonic overprint has produced a highly faulted and structurally complex geological framework, placing significant demands on engineering geological site characterization. While cavern structures should ideally be located within thick, homogeneous strata, the planned tunnels will likely intersect a diverse succession of Paleozoic rock units and multiple fault zones.

ET requirements and related challenges

The successful implementation of the Einstein Telescope is tied to a variety of mainly environmental and geological factors that concern the conceptual design, the layout, and positioning in the subsurface (Fig. 4). A comprehensive conceptual design study compiling the fundamental requirements and main characteristics of a potential site for the ET, including key elements of the research infrastructure, estimated costs and an implementation timeline, was initially conducted by the ET Science Team, (2011) and updated in 2020 by the ET Steering Committee (ET Steering Committee Editorial Team 2020). The current design features an extensive tunnel system that forms an equilateral triangle with sides approximately 10 km in length and outer tunnel diameters ranging from 7.3 to 8.4 m, situated about 250 m below the ground surface (Freise et al. 2009, 2011; Sathyaprakash et al. 2012). At each vertex, large caverns, up to 30 m in height and several tens of meters in length or width, will house key components, including lasers, detectors, cryogenic mirrors, and the required technical equipment.

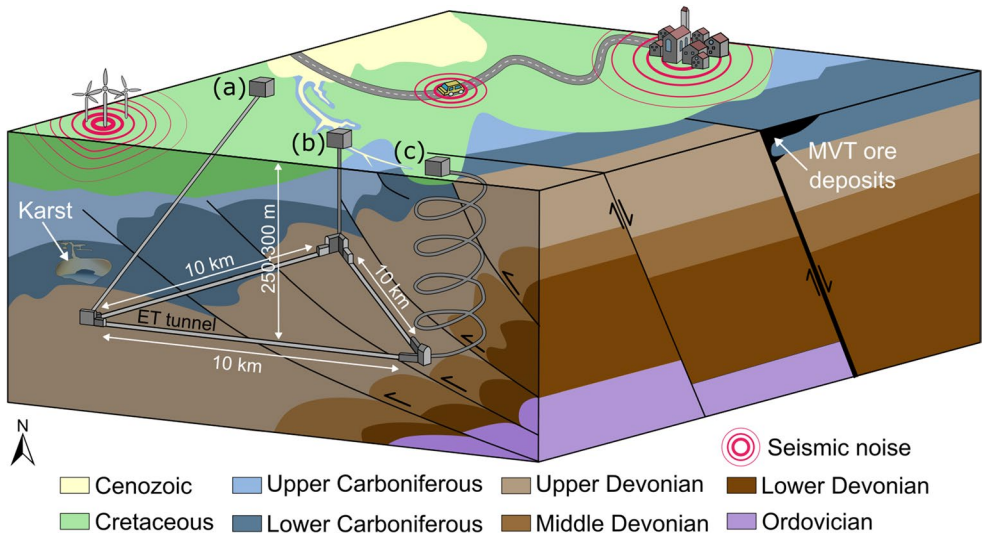

Fig. 4 Conceptual 3D sketch illustrating key geological and anthropogenic factors considered during the site characterization of the Einstein Telescope (ET) in the Euregio-Meuse-Rhine (EMR). The ET infrastructure is schematically shown at a depth of ~250–300 m below the surface. Illustrated are various potential access infrastructure concepts for the ET facilities: (**a**) inclined access tunnels, (**b**) vertical shafts, and (**c**) helical ramps. Major influencing elements include surface noise sources (e.g., traffic, wind turbines, cities), karst zones(e.g. in Carboniferous limestones), and structurally controlled Mississippi Valley-Type (MVT) Pb–Zn ore deposits, mainly localized along normal faults. Thrust and normal fault systems, lithological contrasts, and stratigraphic units are depicted to highlight their relevance for seismic noise propagation and potential future subsurface conflicts. Geological units, structures, and infrastructure are not to scale and are presented in a generalized and conceptual manner

Access to the facility will be provided via shafts, inclined access tunnels, or helical ramps. The depth chosen for the ET, between 250 and 300 m, is a tradeoff between optimal seismic noise attenuation and construction and maintenance cost considerations (Amann et al. 2022). Several critical factors influence the feasibility, cost-efficiency, and scientific potential of a given ET site. These are addressed in the following sections.

Ambient noise characteristics

The delimitation of potential sites for the Einstein Telescope is based on the spatial distribution of different sources of anthropogenic seismic noise and the attenuation effectiveness of geological units. The reduction of seismic noise in a low-frequency band (1–10 Hz) and related Newtonian noise is the primary reason for siting modern gravitational wave detectors below the Earth's surface (Hild et al. 2011). Anthropogenic seismic noise emission in this frequency band is generated from various sources such as wind turbines (WT) and wind parks (WP), road and railway traffic, and industrial activities (Saccorotti et al. 2011; Neuffer and Kremers 2017; Zieger and Ritter 2018; Brenguier et al. 2019; Limberger et al. 2023). Although the amplitude attenuation distance of such noise can span several kilometers (Saccorotti et al. 2011; Zieger 2019), specific geological units can significantly limit seismic wave propagation (Boese et al. 2015; Zieger and Ritter 2018; Limberger et al. 2023). Preliminary seismic and Newtonian noise characterizations were conducted in and around the Terziet borehole, situated at the Dutch-Belgian border within the Euregio Meuse-Rhine area. The results have shown that the characteristic geology of 25–40 m thick, soft Cretaceous and Cenozoic sediments on top of Paleozoic hard-rock sequences is efficient in attenuating surface generated seismic noise by a factor of up to 10^4 at a depth of 250 m (Koley et al. 2019, 2022), diminishing related Newtonian noise below required sensitivity (Bader et al. 2022).

Geological and geotechnical characteristics

The construction of the underground infrastructures requires stable ground conditions, where the choice of appropriate excavation methods and excavation support depends mainly on the rock mass characteristics and geotechnical properties. The spatial distribution and (mechanical) properties of rock mass discontinuities, such as fractures, joints, and fault zones, must be considered for discontinuity-controlled block and wedge failure as well as stress-related deformability processes for cavern and tunnel design. Local stress conditions are closely related to the previously discussed properties, as these define the stability of the access system in weak ground and the likelihood of rock failure in the brittle, hard rock sequence, where tunnels and caverns will be situated.

Rock abrasivity and strength properties significantly influence the cutting performance of tunnel boring machines, as well as the interaction between rock cutting tools and varying rock types, and related excavation costs (Teymen 2020; Jeong et al. 2023). Abrasiveness, in particular, is directly related to the wear rate of cutting tools (Jeong et al. 2023).

Karstic formations represent a significant engineering challenge due to their complex heterogeneity and unpredictable behavior (LaMoreaux 2019). Underground construction in karst can be associated with several potential hazards, including groundwater ingress, seepage, sudden groundwater inrush, subsidence, and cavern collapse (LaMoreaux 2019). Limestone sequences from the Cretaceous, Lower Carboniferous (Viséan), and Upper Famennian (Frasnian) represent potential karst-bearing lithologies. Due to intense folding and thrusting during the Variscan orogeny, these Paleozoic units may occur at tunnel and cavern depths, where karstification could pose significant challenges. Additionally, karst features in Cretaceous strata may impact the design and placement of access infrastructure.

Hydrogeological characteristics

The drainage requirements for the subsurface infrastructure will be primarily governed by the hydrogeological properties of the rock mass, including hydraulic conductivity, porosity, storativity, hydraulic head differences, the source of inflows, and their transient behavior. Groundwater inflows must be carefully considered during both construction and operational phases, as they can disrupt activities and introduce additional noise (Masset and Loew 2010; Farhadian and Nikvar-Hassani 2019). Inflow volumes can vary widely, especially in fault zones and karstified regions, where magnitudes may differ by several orders (Amann et al. 2020). Drainage systems themselves may contribute to seismic noise through the operation of machinery and water movement within rock fractures (Akutsu et al. 2018; Amann et al. 2020). The construction of access facilities, tunnels, and caverns may intercept two key aquifers:

(a) The Cretaceous formations form a hydraulically connected aquifer system with high recharge potential and permeability, particularly in the Gulpen and Aachen Formations. These units contribute significantly to regional groundwater flow, but may present challenges due to local karst development and vulnerability to surface contamination, especially where formations are eroded or faulted (Laloux et al. 2000);

(b) Paleozoic aquifers comprise both confined and unconfined water-bearing units, typically within folded rock strata and fault zones. While most Paleozoic rocks (e.g., shales and siltstones) possess low permeability; fractures, fault zones, karstified carbonates, and in to minor extend sandstones, exhibit high hydraulic conductivities, making them critical features in hydrogeological assessments (Laloux et al. 2000).

Socio-economic criteria

The construction of ET infrastructures, extending over several decades, will have significant and lasting impacts on the surrounding environment. Vibrations from heavy machinery, dust, spoil disposal, and the use of water and groundwater are just a few factors that can affect the local and regional environment.

Socio-economic suitability and public acceptance are closely linked to environmental preservation and protection (Amann et al. 2020). Compliance with applicable directives at the national and EU legal levels for preserved natural areas can have various implications for construction projects such as the ET. In Europe, the interconnected network of areas dedicated to preserving species and habitats, collectively recognized as Natura 2000, is of significant importance (European Union 2019). In these areas, construction activities may be restricted under Article 6 of the Habitats Directive (92/43/EEC). Compatibility assessments for designated Special Areas of Conservation (SAC) and Special Protection Areas (SAP) can determine the feasibility of infrastructure development.

The construction of ET infrastructures may impact regionally significant groundwater resources, particularly the two major aquifer systems currently in use, both of which are sensitive to disturbance and are hydrologically interconnected with surface and subsurface flows.

Additionally, parts of eastern Belgium are known to host Mississippi Valley-Type (MVT) Pb-Zn deposits. These deposits formed as a result of hydrothermal mineralization within the Lower Devonian and Early Paleozoic basement rocks, with mineralizing fluids ascending along SE–NW-trending normal faults during post-Variscan tectonic activity linked to the European Cenozoic rift (Dejonghe 1998; Evrard et al. 2018; Bevandić et al. 2020). Mineral precipitation was further influenced by lithological contrasts, with mineralization preferentially occurring where permeable carbonates were bounded by less permeable shales or sandstones (Evrard et al. 2018). Any future subsurface exploitation in these structurally and lithologically favorable zones could pose a conflict of interest, and future mining activity could be a potential source of underground noise, both of which are critical considerations for the planning and operation of the ET.

Scope of investigations

The investigations conducted in the present study aim to provide a preliminary characterization of the Euregio-Meuse-Rhine (EMR) area, thereby contributing to feasibility assessments and the identification of optimal siting conditions for the Einstein Telescope. A general workflow of the applied work steps is illustrated in Fig. 5.

Desk study

The perimeter of the potential area suitable for the planning and construction of the ET was defined based on geographical information systems (GIS) with special emphasis on:

i. Geological conditions such as noise attenuating soft sequences and major fault zones;

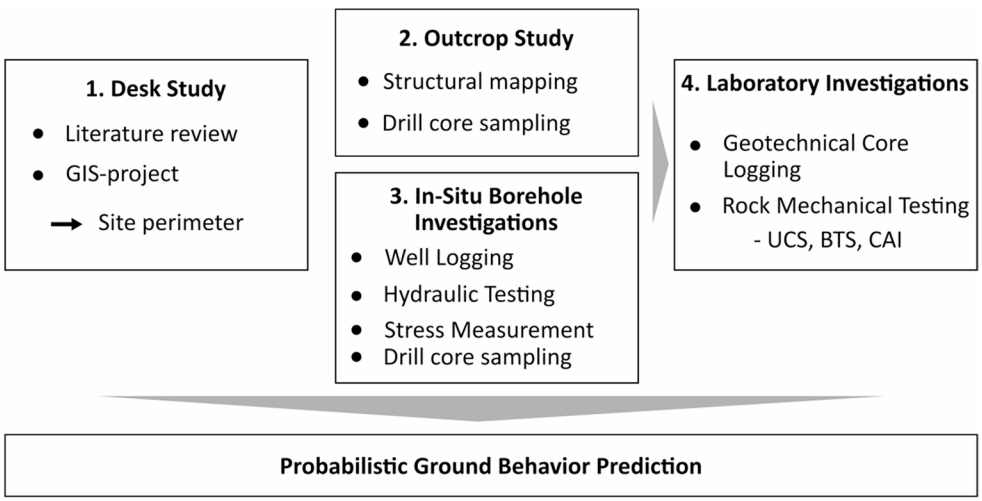

Fig. 5 Simplified workflow of general work packages conducted for the present study. Uniaxial compressive strength = UCS, Brazilian tensile strength = BTS, Cerchar abrasiveness index = CAI

ii. Sources of seismic anthropogenic noise (such as wind turbines, busy roads, railways);
iii. Natural preservation areas.

Buffer zones were established around potential sources of seismic noise. A perimeter of 5 km was chosen for wind turbines based on literature values (Saccorotti et al. 2011; Zieger 2019).

Outcrop study

Geological, geotechnical, and structural data of the Paleozoic rock masses as the prime target were gathered from seven outcrops for first estimations on the overall rock mass appearance with special emphasis on:

a. Occurrence, frequency, and spatial orientation of fractures;
b. Basic rock mechanical properties.

Schmidt Hammer rebound tests (SH) were carried out on all outcrop walls. Various basic rock mechanical tests were performed on cylindrical rock samples drilled from the outcrop faces,. Point load tests (PLT) were conducted following the standard of the German Society of Geotechnics (DGGT) (Thuro 2010). These tests are equivalent to those specified by ISRM. Uniaxial compressive strength values (UCS) were calculated from the derived point load indices (I_s). The outcrops investigated for this study are marked in Fig. 1. Basic outcrop information and the respective methods applied are given in Table 1.

In-Situ investigations

Three 250 m deep boreholes, were drilled within the siting region. The Cottessen-1 borehole (Cot-1) was drilled between October and December 2021. A water-flushed triple tube core barrel was used to create a 252.8 m deep borehole with a diameter of 146 mm. Non-oriented drill cores with a diameter of 101 mm were continuously retrieved from approximately three metres below ground level. A second borehole (Ban-1) was drilled between August 2021 and January 2022 in the Dutch municipality of Banholt (Limburg). The uppermost ~ 130 m were drilled by using wet rotary drilling. Borehole cuttings were sampled every metre. Coring was conducted between 130 m and 252 m. In the summer of 2023, a third borehole in the vicinity of the Wallonian municipality of Aubel was drilled (Aub-1) using a down-the-hole hammer (DTH) from 0 to 150 m and double-tube core drilling from 150 to 250 m. After drilling, a geophysical well logging campaign was carried out in all boreholes, including optical borehole televiewers (OPTV) and acoustic borehole televiewers (ATV), natural and spectral gamma logs, and formation resistivity logs.

Hydrogeological borehole properties were investigated using straddle double packer systems in a well-testing campaign. The test methods applied in different depth intervals comprise pulse and slug tests, as well as injection tests with a constant pumping rate. Vertical distributions of hydrogeological properties (hydraulic conductivity (K) for the borehole depths were established. Single and double packer intervals were tested at various depths, depending on the borehole conditions. Hydraulic stress measurements (hydraulic fracturing (HF) and hydraulic testing of pre-existing fractures (HTPF) were performed within the Cot-1 borehole to evaluate local stress conditions following ISRM standard recommendations (Haimson and Cornet 2003). Spatial analysis of the newly formed or propagated fractures was conducted to determine stress directions using acoustic televiewer data.

Table 1 Outcrop information of the investigated daylighting rock sequences and overview of the applied investigation methods for each outcrop. SH = Schmidt Hammer, PLT = Point load Test

#	Coordinates	Age	Formation	Rocktype	Applied Investigation			
					SH	PLT	Structural mapping	Photo-grammetry
7	50°48’44"N 6°06’22"E	Westphalian	Houiller (Westphalian A[*a])	Sandstone	✓	✓	✓	✓
6	50°44’14"N 5°57’44"E	Namurian	Houiller (Namurian A[*a])	Alternating Sandstone /Claystone sequences	✓	✓	✓	✓
5	50°42’43"N 5°41’12"E	Viséan	x	Limestone	✓	✓	✓	x
4	50°39’21"N 6°01’46"E	Viséan	x	Limestone	✓	✓	✓	x
3	50°39’33"N 6°01’42"E	Tournaisian	Landelies - B.R.b.	Dolomite	✓	✓	✓	x
2	50°42’01"N 5°48’01"E	Famennian	Condroz-Group	Alternating Sandstone /Siltsone sequences	✓	✓	✓	✓
1	50°43’27"N 5°43’08"E	Frasnian	Lustin (Frasnes Limestone[*a])	Limestone	✓	✓	✓	x

[*a]German nomenclature

Laboratory investigations

In a laboratory-based study, geotechnical core logging was conducted, comprising evaluations of rock core qualities (e.g., Rock Quality Designation index values (RQD). Basic rock mechanical testing (UCS and BTS) was conducted on outcrop samples and samples from the Aub-1 and Cot-1 boreholes following the standard proposed by DGGT (Lepique 2022; Mutschler 2022). Abrasiveness values were determined for outcrop and Cot-1 samples on rough-cut and broken surfaces by applying Cerchar abrasiveness index tests (CAI) following the DGGT suggested method (Käsling and Plinninger 2022). Mechanical and abrasiveness tests were performed at the Chair of Geotechnical Engineering and the Institute of Geomechanics and Underground Technology at RWTH Aachen University.

Probabilistic ground behavior model

A preliminary probabilistic ground behavior prediction for a potential ET layout was established in accordance with the directive for the geotechnical design of underground excavations with cyclic and continuous excavation (ÖGG 2021). The geotechnical and hydrogeological data derived from the investigations described above served as input for the model. The geological sequences likely to be penetrated by the individual tunnels were modeled using the open-source geological modeling software Gempy (De La Varga et al. 2019). Through the input of surface points (e.g., stratigraphic boundaries) and orientation data (e.g., outcrop measurements), a surface-based model was first built. Secondly, the stratigraphy at each coordinate of the tunnel trajectories was extracted. The model is based on the aforementioned boreholes, Aub-1, Ban-1, and Cot-1, as well as existing boreholes studied during the desk study. Stratigraphic units were simplified into groups of undifferentiated "Cretaceous", "Carboniferous", and "Devonian" rocks. The fault zone geometries for thrust faults are variable, with dips ranging from 5° to 80°. In contrast, normal faults associated with the Lower Rhine Graben predominantly show a steep (sub-)vertical dip (Cambier and Dejonghe 2012). For simplification, NE-SW striking thrust faults (assumed association with the Variscan orogeny) were implemented with a dip at an angle of 50° towards SE, while NW-SE striking normal faults (assumed association with the rifting of the Lower Rhine Graben) dip at an angle of 90°. Fault zones were assigned a thickness of 10 m for the fault core, while the damage zones on each side of the fault were assumed to be 50 m wide (110 m total width). Given this information, relevant intersecting faults were linearly interpolated at the target depth (Chudalla et al., in prep.).

Results

Area mapping and perimeter

The evaluation of a constrained site perimeter for investigations conducted as part of this study was achieved using geographic information systems (GIS), with a special emphasis on sources of ambient anthropogenic noise, noise-attenuating soft geological units (Cenozoic and Cretaceous), the spatial extent of tectonic fault zones, and natural preservation areas. The results are presented in the maps shown in Fig. 6.

Within the area of investigation, Cenozoic sediments govern most parts of Southern Limburg (NL). These sediments overlie Cretaceous strata that dominate the northern part of the mapped area in Belgium. The Cretaceous pinches out towards the southeast and is limited to a southwest-northeast trending line, roughly traceable along the cities of Verviers, Chaineux, Welkenraedt, and Montzen (Fig. 6a). In part, rivers such as the Guelle in the area of Kelmis carved and eroded the Cretaceous cover, exposing the Paleozoic basement. The same applies to the area South of Aubel and Blegny. Geological fault zones of different tectonic origins and nature spread across the mapped area (Fig. 6c). They show two major trends. Thrust faults such as the Aachen thrust show a SW-NE strike, while normal faults strike predominantly SE-NW. SAC and SAP areas of the Natura 2000 network cover areas in Belgium, the Netherlands, and Germany but mainly focus on the Dutch area of South Limburg and the southeastern parts of the mapped Walloon region (Fig. 6d). Sources of potential ambient anthropogenic noise cover wide parts of the mapped area (Fig. 6c). Traffic arteries mainly connect the three urbanized regions of Aachen, Maastricht and Liège. The European route 40 (E40) connects the cities of Aachen and Liège. A polyhedral area between the major traffic pathways is crosscut by a W-E trending, frequently used cargo railway. The HSL3 (French LGV3) high-speed railway between Aachen and Liège largely follows the E40. Single wind turbines (WTs) and wind parks (WPs) are strongly related to low ambient seismic noise emissions in the frequency band of 1–10 Hz. While single WTs are few within the mapped area, WPs align especially along the German-Dutch and German-Belgian borders, northwest and south of Aachen.

Following these investigations, the preliminary results suggest that Dutch Southern Limburg, the Northern part of the Walloon region, and Flanders are the most suitable areas in that Limited seismic noise sources are extensively covered by an attenuating geological cover of soft Cenozoic and Cretaceous age formations.

The Einstein Telescope layout used in this study aimed to fulfill both criteria while avoiding major fault zones and

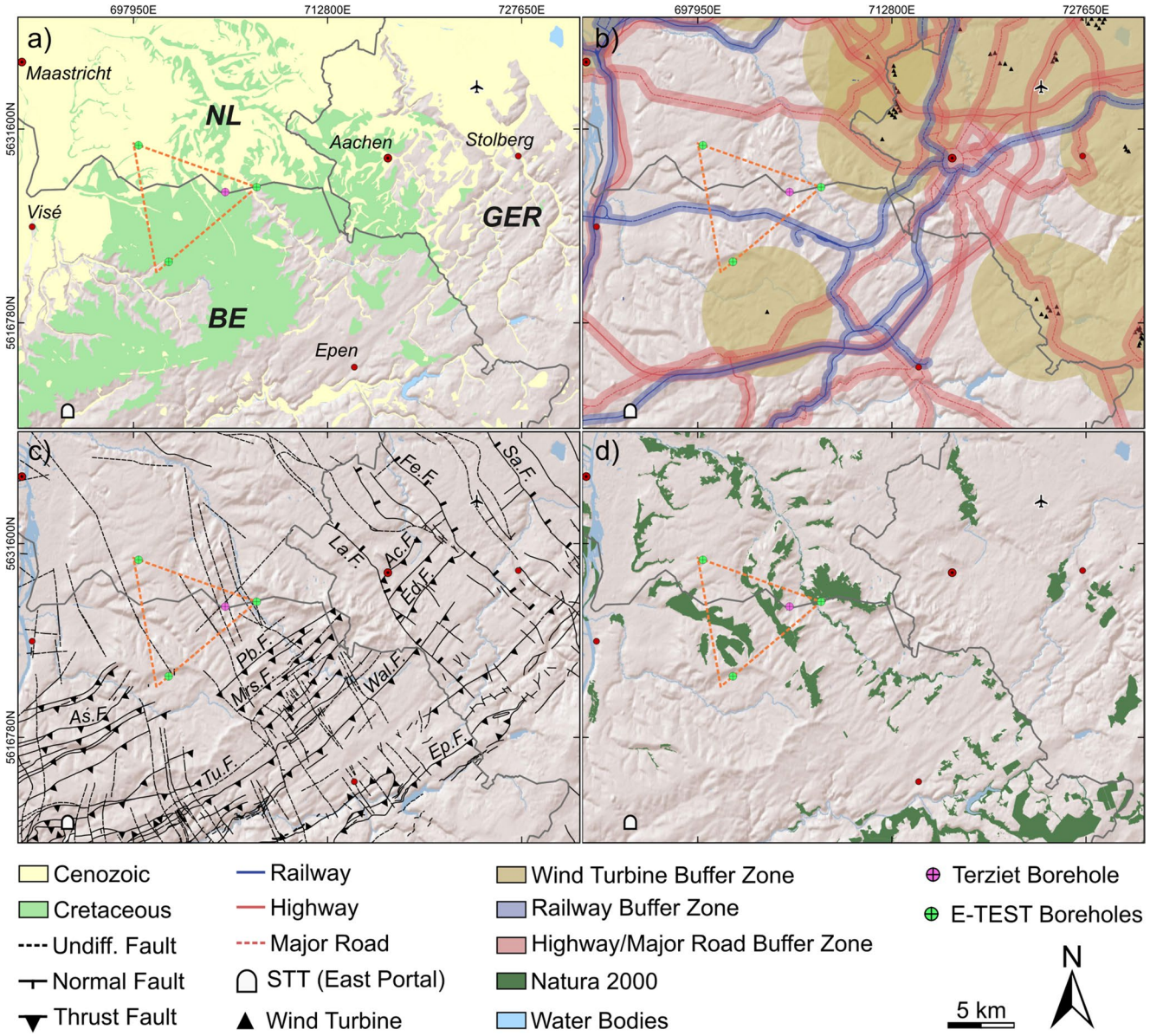

Fig. 6 Results of the EMR GIS mapping campaign with thematic maps related to different important ET site characterization criteria: (**a**) Spatial extension of noise dampening Cretaceous and Cenozoic rock and soil units; (**b**) Major sources of anthropogenic noise with buffer zones; (**c**) Mapped major fault zones (undifferentiated) (**d**) Nature conservation areas in accordance to the Natura 2000 classes Special Areas of Conservation (SAC) and Protection (SPA). Fault zone abbreviations: As.F. = Asse Fault, Tu.F. = Tunnel Fault, Ep.F. = Eupen Fault, Wal.F. = Walhorn Fault, Mrs.F. = Morsenet Fault, Pb.F. = Plombières Fault, La.F. = Laurensberger Fault, Ac.F. = Aachen Fault, Ed.F. = Eilendorf Fault, Fb.F. = Feldbiss Fault, Sa.F. = Sandgewand Fault

considering borehole locations, thereby providing a meaningful dataset for future siting considerations.

Outcrop study

Seven outcrops with rocks of variable age and lithology were studied. Cylindrical samples were drilled horizontally from the rock faces of all outcrops for basic rock mechanical tests. Investigated outcrops of Upper Devonian, Lower Carboniferous, and Upper Carboniferous age are shown in Fig. 7. Representative cored samples are also presented. The geotechnical in-situ data from Schmidt Hammer and Point Load Tests are summarized in Table 2.

Frasnian limestones outcrop in an abandoned quarry near the municipality of Dalhem (BE). They exhibit an irregular assemblage of discontinuities, resulting in the formation of polyhedral blocks. Due to this random distribution, no prominent spatial orientation could be derived. Drilled samples show frequent recrystallized calcite veins on a centimeter scale and thicknesses between millimetres to a

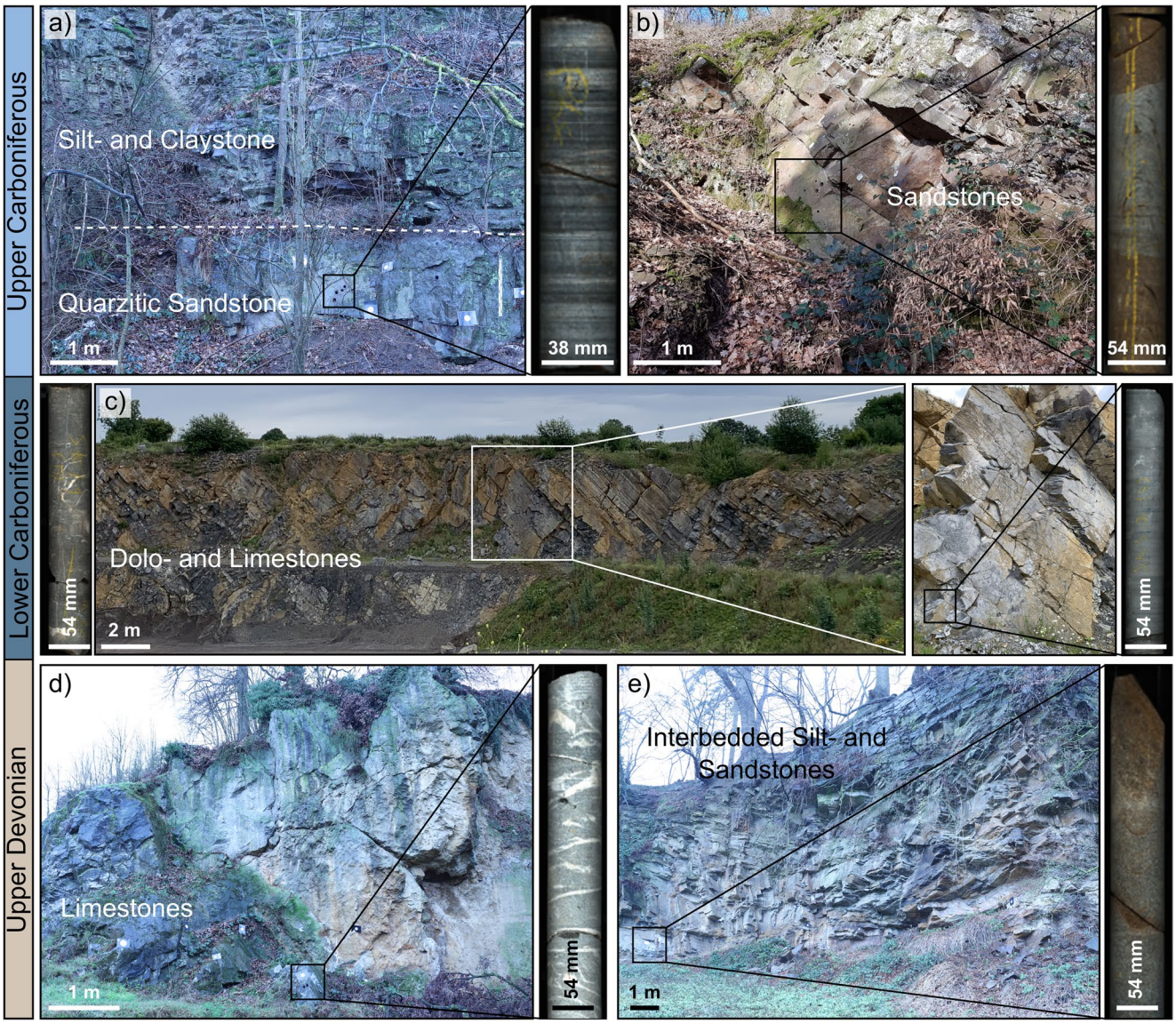

Fig. 7 Outcrops with daylighting rocks of variable age investigated for this study with exemplary drill core samples of: (**a**) Namurian cross-bedded sandstone-siltstone-shale sequences in Plombières (BE); (**b**) Westphalian, weathered sandstones in the Wurm valley (GER); (**c**) Outcrop wall of the Carnol quarry (BE) with bedded dolo- and limestones of Tournaisian and Viséan age; (**d**) Frasnian limestones close to the municipality of Dalhem (BE); (**e**) Sand- and siltstone alterations of the Famennian Condroz Group from a roadcut in vicinity of the Val-Dieu abbey (BE)

few centimetres (Fig. 6d). Schmidt Hammer rebound values (SRV) indicate high mean UCS values of 170 MPa, while the mean UCS derived from point load tests (PLT) suggests a lower UCS of 106 MPa.

Upper Devonian sandstone-siltstone alterations of the Famennian Condroz Sandstone Group outcrop in a road cutting close to the Abbey of Val-Dieu (BE) (Fig. 7e). The approximately 1 m thick sandstone beds show frequently interbedded silt- and claystone layers. Discontinuities are traceable on a decimetre-to-metre scale, resulting in a blocky outcrop appearance. The spatial orientations of discontinuities were determined using a photogrammetric model. The most prominent discontinuity set shows an overall WNW-ESE strike, a moderate dip towards the North, and is interpreted as bedding. Two additional joint sets, with overall NW-SE and NE-SW directions, dip at 79° and 75°, respectively, and cross-cut the bedding. Lower hemisphere Schmidt projections display the mean spatial orientation of these sets (Fig. 8b). Both the Schmidt Hammer and PLT indicate very high UCS values exceeding 200 MPa.

Lower Carboniferous dolostones and limestones outcrop within the Carnol quarry near Kettenis (BE) (Fig. 7c). SW-NE striking, bedding parallel discontinuities spaced at approximately 1 m, dipping at a mean of 48° towards SE. The

Table 2 Summary of geotechnical outcrop investigations. The stated UCS values were derived from the respective investigation method. LSt = Limestone, SSt = Sandstone; Dst = Dolostone, SD = Standard deviation, Nb. = Number of conducted tests, Uniaxial compressive strength (UCS^{*a}) calculated from Schmidt Hammer rebound values (SRV) and UCS^{*b} calculated from point load tests (PLT)

#	Age	Lithology	SRV				I_S [MPa]				
			Min.	Max.	Mean ± SD	Nb.	UCS^{*a} [MPa]	Min.	Max.	Mean ± SD	Nb.	UCS^{*b} [MPa]
7	Westphalian	Sst	43	69	56 ± 7	30	165	3	16	8 ± 4	9	191
6	Namurian	Sst	50	77	66 ± 7	30	> 200	3	13	9 ± 3	6	203
5	Viséan	Lst	28	60	44 ± 10	31	115	2	5	4 ± 1	6	87
4	Viséan	LSt	30	76	55 ± 11	33	188	5	9	7 ± 1	8	155
3	Tournaisian	Dst	36	68	55 ± 8	30	196	2	6	4 ± 1	11	98
2	Famennian	Sst	44	77	63 ± 8	30	> 200	8	14	11 ± 3	2	260
1	Frasnian	LSt	39	69	54 ± 10	30	170	2	6	4 ± 1	10	106

steep dip reflects intense Variscan folding. A SW-NE striking, joint set that shows a NW-directed 52° mean dip cuts the bedding parallel discontinuities almost perpendicularly. Rock strength, as indicated by the Schmidt Hammer and PLTs, is considered high, with calculated mean UCS values of 188 MPa and 155 MPa, respectively. Detailed lithostratigraphic interpretations of the Carnol quarry are given by Poty (2016).

Viséan limestones investigated on an outcrop southwest of the municipality of Richelle (BE) indicate SRV and PLT-based UCS values of 115 MPa and 87 MPa, respectively. However, structural measurements of discontinuities were not possible due to dense vegetation.

Cross-bedded sandstones and claystones, outcropping on a steep, SE-dipping rock face within the municipality of Plombières, represent parts of the Namurian sections of the Houiller Group (Walter 2010) (Fig. 7a). The outcrop displays a strongly folded synclinal structure. In the southern part of the outcrop, the synclinal hinge is exposed, as indicated by the nearly horizontal orientation of the bedding. Samples were taken from the southern outcrop area, where persistent bedding parallel discontinuities are spaced at between 70 cm and 100 cm. Their spatial orientation is almost horizontal, with a very slight dip of ~2° towards the southeast. Occasional subvertical discontinuities with an 82° mean dip towards ESE (110° mean dip direction) are present. The strength of the sandstone is very high (> 200 MPa), as determined by both Schmidt Hammer and PLT tests.

Within the Wurm valley, South of Würselen (GER), the brownish-weathered sandstone beds of the Westphalian dip steeply towards the southeast (Walter 2010) (Fig. 7b), and bedding-parallel joints (J2) are spaced at 50–100 cm. The bedding is cross-cut by two distinct joint sets, of which one dips with a mean dip of 78° towards WSW (J1), while the other set strikes SE-NW and dips at 65° towards NE (J3). Schmidt Hammer and PLT results indicate high rock strength of 165 MPa and 191 MPa, respectively.

Borehole characteristics

The Aub-1, Ban-1, and Cot-1 boreholes were investigated using several in-situ methods, including geophysical well logging, hydraulic packer tests, and hydraulic stress measurements. Sample material was retrieved as cuttings and/or drill cores. The reported lithologies are derived from natural gamma ray, resistivity, and sonic-wave-velocity logs as well as cutting and core logging. Lithostratigraphic borehole profiles, along with the gamma ray logs (GR), are given in Fig. 9.

Aubel-1

Based on cuttings and core logs, the uppermost 20 m of the Aub-1 borehole consisted of Namurian shale. From 20 m

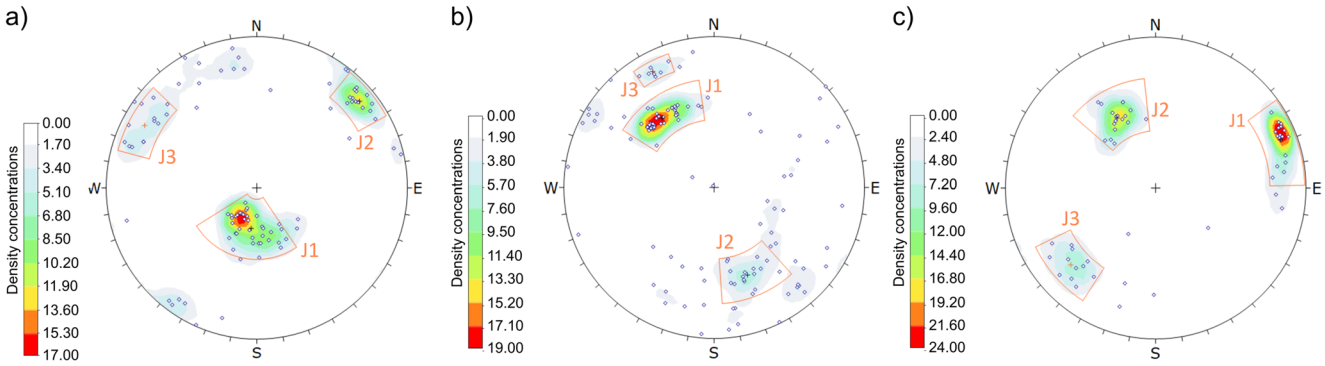

Fig. 8 Lower hemisphere equal area projections of the major discontinuity sets from: (**a**) the Val-Dieu road cut (BE); (**b**) the Carnol quarry (BE); (**c**) Westphalian sandstones within the Wurm valley (GER). Data for (a) and (c) was generated with a photogrammetric survey, while the spatial data for (b) was taken via scan-line mapping

to 27 m, a brecciated interval marked the transition to the Lower Carboniferous. This was followed by light grey limestone, attributed to the Viséan, extending to a depth of 45 m. Between 45 m and 50 m, a shale unit indicated the onset of Upper Devonian strata. Well-logging was performed from 150 m below ground level, where gamma ray logs indicated an alternating sandstone-siltstone-shale sequence, with GR readings varying on a decimetre-to-metre scale (Fig. 9a). Stratigraphically, the logged borehole section was assigned to the Upper Devonian (Famennian) Montfort Formation. Structural discontinuity mapping was performed based on optical and acoustic televiewer data. Three distinct discontinuity sets were revealed, of which the most prominent set is interpreted as bedding with a moderate dip towards SE and a mainly SW-NE strike. Bedding parallel open joints occurred throughout. A second, steeply dipping discontinuity set strikes NNE-SSW, and a third strikes WSW-ENE. A general decrease in fracture density was observed with depth.

The core material retrieved from Aub-1 showed mostly good rock quality with RQD values mainly > 75%, but poor quality core (RQD < 50%) was present from 149.7 m to 154.7 m and from 166.77 m to 172.7 m, potentially corresponding to two minor fault zones.

Banholt-1

The Ban-1 borehole was drilled with a metal casing from ground level to a depth of approximately 200 m to maintain ground stability. Well logs are limited to the lowermost 50 m. Geological interpretations of the upper 200 m are limited to the natural gamma ray readings, cuttings, and drill cores. A zone of moderately compacted soil within the uppermost 21 m was followed by light greyish to yellowish, flint nodule-bearing chalk between 21 m and 43 m. From 43 m downwards, a gradual color shift to darker greyish/greenish and a slight increase in gamma readings indicate a progressive increase in glauconite content. Glauconitic, greenish marls with a large number of belemnite fossils at a depth of 62–63 m resulted in a distinct GR peak. Dark greyish to dark greenish marly rock units dominated the borehole lithology down to a depth of 138 m. Representative cutting samples from various depths are presented in Fig. 10. The lithological succession between 21 m and 138 m is interpreted as part of the Cretaceous Gulpen formation. Between 138 m and 146 m, varying GR values (ranging from ~20 to 79 API) indicated sandy-silty alterations, and the drill cores were of poor quality, with frequent core losses in a centimetre-to-metre range. Preserved core segments revealed greenish-colored, muddy siltstones between 138 m and 140 m, and coarser-grained, greyish to brownish siltstones and sandstones between 140 m and 142 m. Chemical reactions with hydrochloric acid indicated a slight to moderate carbonate content. Core segments of brown, sandy conglomerate appeared between 143 m and 144 m. The borehole section between 138 m and 145 m was assigned to the Cretaceous Vaals formation (Bless et al. 1986; Walter 2010). Below this, a distinct increase in the gamma-ray readings (up to 327 API) indicated the transition to a shaly rock, and cores between 146 m and 148 m showed a color transition from pale red to dark grey (Fig. 10b).

Below 152 m, moderately fractured dark grey to black cores were present. Brown staining, typical of that produced by weathering of pyrite and pyrite concretions, was present in places throughout the shales. Coal seams were present in places. The borehole section between 148 m and the bottom hole is interpreted as part of the Upper Carboniferous Baarlo Formation.

Acoustic borehole televiewer logs (ATV) showed a major trend of S-N striking discontinuities with a shallow E-wards dip, which is interpreted as bedding. A second discontinuity set with a steeper W-ward dip was spaced at approximately 1 m. The fracture density varied between 0 and 14 fractures/m with a mean of 4.7 fractures/m. The clayey nature of the rock led to the rapid formation of drying-induced cracks

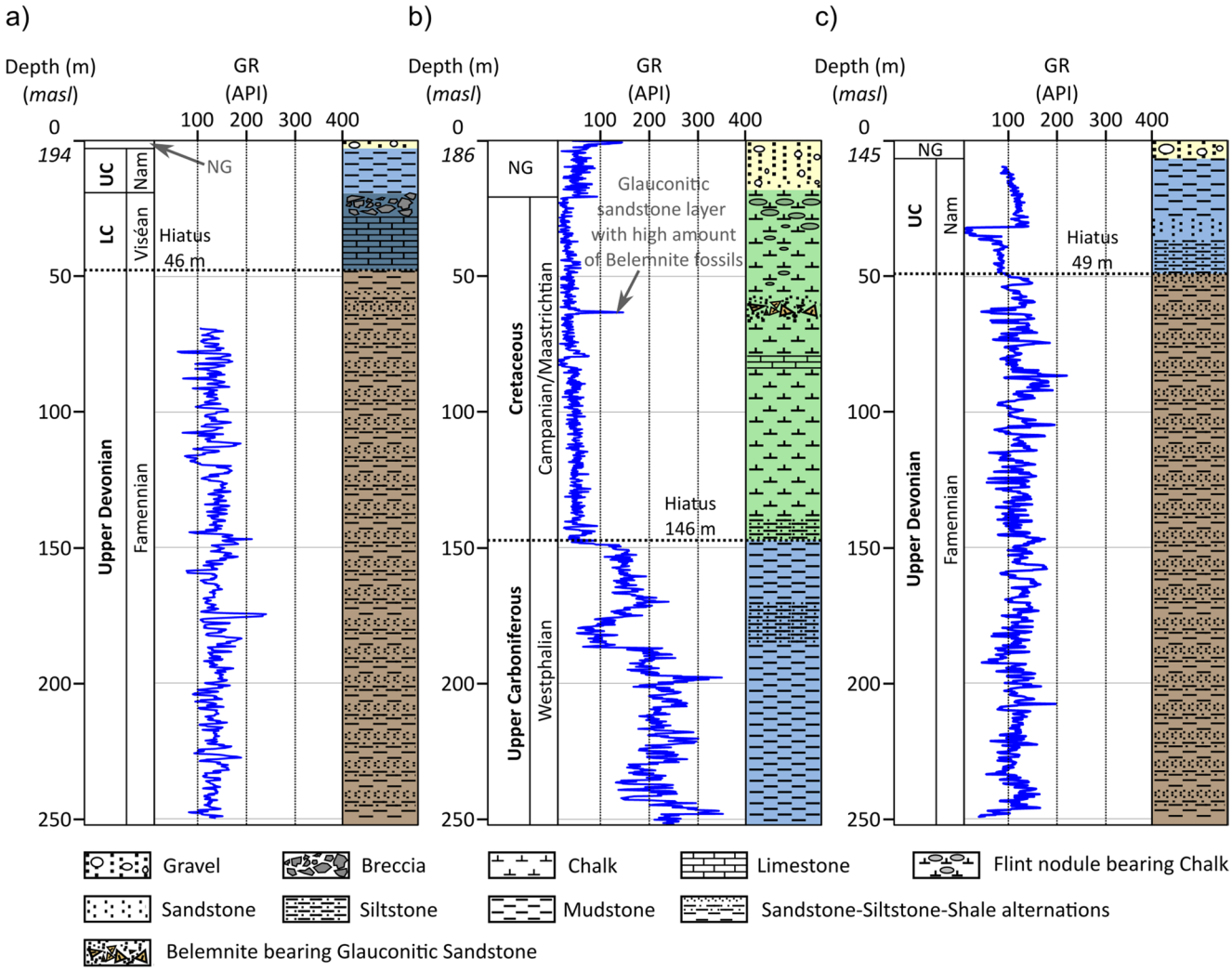

Fig. 9 Lithostratigraphic borehole profiles and GR signals of the borehole (**a**) Aub-1, (**b**) Ban-1, and (**c**) Cot-1. Italic numbers on the depth scale give the total elevation of the respective borehole location in meters above sea level (masl). LC = Lower Carboniferous, UC = Upper Carboniferous, NG = Neogene

and fractures, mostly occurring parallel to each other. Rapid swelling and gypsum precipitation led to significant material decomposition in certain core sections. RQD values varied throughout the core run, with a mean of 47%, which is considered poor. The fragile nature of the cores prevented the collection of samples suitable for mechanical rock testing. Anyhow, Schmidt hammer rebound values ranging from 8 to 44 indicated potential Uniaxial compressive strengths of between 15 MPa and 55 MPa, with an assumed rock unit weight of 26 kN/m^3.

Cottessen-1

The Cot-1 borehole encountered loose surficial sediments within the upper three metres, underlain by weathered and disintegrated bedrock. From this point down to approximately 31.7 m depth, the lithology comprised homogeneous grey-black shale, displaying a subtle coarsening-upward trend as suggested by the gamma ray log. A transition to grey, strong sandstone resulted in a distinct gamma ray drop to a minimum value of 2 API. Quartz-filled veins were present in places. Between 35 m and approximately 49 m, a sandy shale lithology was predominantly present. The stratigraphic interval between 3 m and 49 m in the borehole is attributed to the Namurian (Walter 2010). Between 35 m and 49 m, the bedding dipped at ~17° towards the South. From 49 m down to the final depth of 251 m, the Cot-1 borehole was drilled through sandstone-siltstone alterations, partly intersected by shale layers. Gamma ray readings indicated distinct lithological changes on a small centimetre to metre scale. The alternating sandstone-siltstone lithology was interpreted as part of the Upper Famennian Condroz Group, with bedding planes exhibiting a SW-NE strike and a mean dip of approximately 15° towards the southeast.

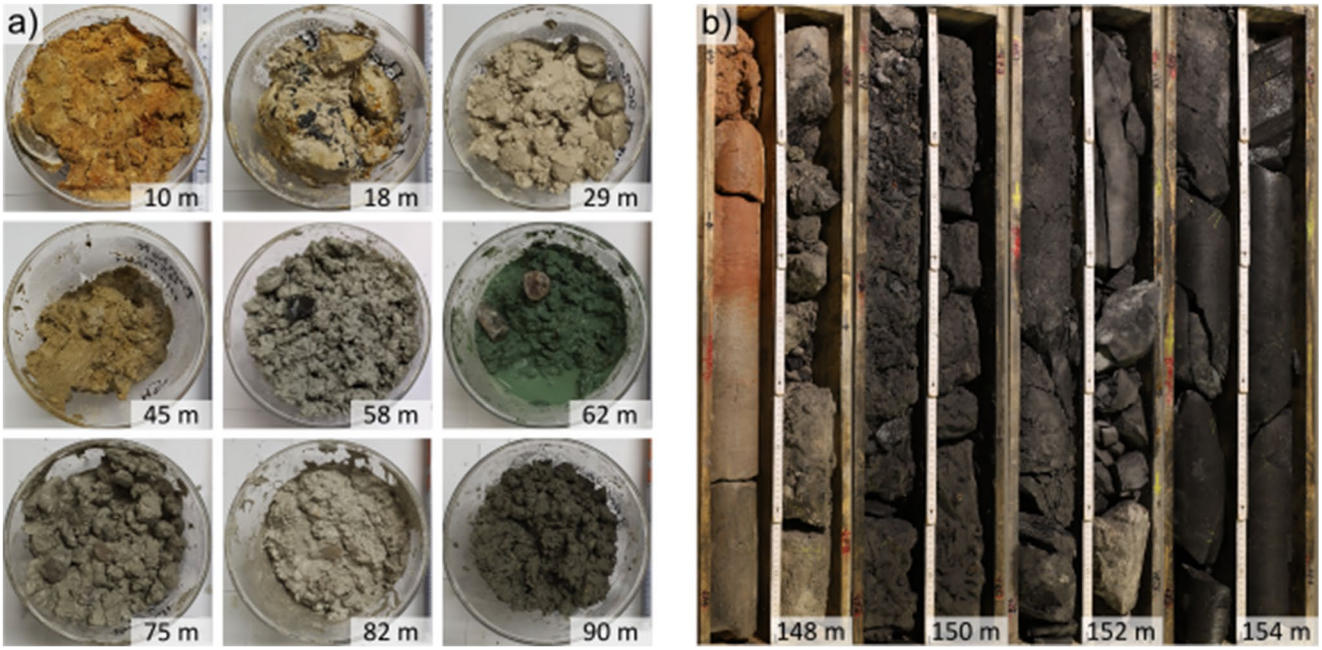

Fig. 10 (**a**) Cutting samples from the Ban-1 borehole. Samples between 18 m and 90 m are assigned to the Cretaceous Gulpen Formation. At approximately 62 m a layer of glauconitic, green sandstone contains many Belemnite fossils. (**b**) Drill cores from the Ban-1 borehole show a clear transition of lithologies

The rock mass penetrated by the Cot-1 borehole was highly fractured with partly > 10 fractures/m (e.g., 177–178 m) and an opening width of up to several decimetres (e.g.,~ at 73 m). Joints occurred predominantly along bedding planes. Additionally, two distinct joint sets occurred throughout the borehole run, both of which show a SE-NW strike, with one dipping 62° towards NE and the other 74° towards SW.

The integrity of the extracted rock cores was highly variable, with joints, faults, and other fractures occurring irregularly along the borehole's length. While two predominant joint sets were identified, the distribution of fractures was discontinuous and unpredictable in depth, resulting in widely varying RQD values that ranged from excellent to very poor, but predominantly indicated poor to fair rock quality. With an RQD-mean of 50% from the individual values, the rock mass was transitional between poor and fair rock quality. The results of RQD evaluations from all boreholes are summarized in Fig. 11, where the individual RQD categories are plotted against their frequency of occurrence. Figure 12 provides an overview of spatial discontinuity properties from all three boreholes, derived from acoustic and optical borehole televiewer data.

Hydrogeological conditions

Existing hydraulic data from pumping and infiltration tests conducted mainly in shallow wells penetrating Cretaceous, Carboniferous, and Devonian strata (Laloux et al. 2000) were available for the Walloon part of the wider E-TEST area and the Soumagne train tunnel on the Brussels-Cologne high-speed train line SW of the E-TEST area. The Soumagne tunnel data were derived from hydraulic tests conducted in geotechnical pre-drillings and estimates of water inflow into the tunnel shortly after excavation, and are restricted to the Carboniferous units (Janssens et al. 2005).

Estimating mean values for hydraulic parameters is unreliable due to the limited amount of data obtained and the preferential siting of wells in permeable formations, including intersections of multiple faults, fault zones, and fracture zones, therefore, only ranges of transmissivities/hydraulic conductivities are quoted. The shallow depth of the wells prevents any trend with depth from being revealed. The hydraulic properties of the Cretaceous cover rocks depend on:

i. the degree of fracturing of consolidated sediments such as the chalks of the Gulpen Formation with transmissivities of between 1×10^{-3} m²/s in fractured chalk and 1×10^{-5} m²/s in intact rock;
ii. the proportion of fine-grained sediments such as silt and clay in the sequence, with transmissivities of 1×10^{-5} m²/s for clay- or silt-rich sediments and 1×10^{-4} m²/s for sandy formations.

In comparison, the transmissivity of Paleozoic rock is predominantly dependent on the degree of fracturing and karstification of carbonate rocks. Karstified Carboniferous limestone yields transmissivities of up to 3×10^{-1} m²/s.

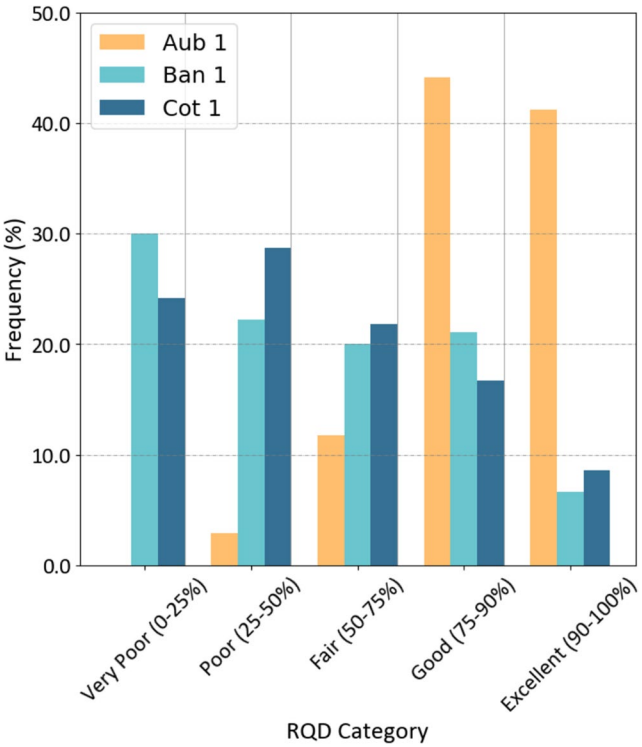

Fig. 11 Rock quality designation (RQD) category distributions of the investigated boreholes. While the boreholes Ban-1 and Cot-1 show frequent drill cores of very poor and poor quality, the cores retrieved from the Aub-1 borehole can generally be considered of good quality

Fractured but unkarstified limestone, fractured shales, and sandstones yield transmissivities of between 6×10^{-7} m²/s and 3×10^{-3} m²/s. Increased transmissivities have also been observed along fractures. High inflows, correlated with lineaments inferred from high-resolution digital elevation models (DEM) at the surface-projected Soumagne tunnel trajectory, also roughly correlated with main valleys, suggesting a strong link between subsurface fractures, surface topography, and water flow paths. Inflows of up to 1.5 m³/m/h were recorded, correlating with hydraulic conductivities between 2×10^{-6} m/s and 1×10^{-5} m/s. The records were truncated at a minimum inflow rate of approximately 6×10^ (−2) m³/m/h, corresponding to 1×10^ (−8) m/s.

The three boreholes, Cot-1, Ban-1, and Aub-1, were tested hydraulically using a double-straddle packer system in multiple intervals. The results are plotted against the respective depth of the test interval in Fig. 13. The Cottessen borehole was sited some 30 m above the ENE-WSW oriented valley of the torrent Cottesserbeek. The sharp valley flank continues beyond the tributary to the Gueule River. The borehole logs indicate that the primary orientation of discontinuities, such as faults and fractures, strike NE-SW, which correlates with the orientation of the Cottesserbeek Valley and its Westward continuation. Thus, hydraulic conductivities of 6×10^{-7} m/s to 1×10^{-5} m/s estimated analytically by curve matching and straight-line approximations from slug and active/passive phases of injection tests for the Devonian sandstones and siltstones represent conditions from a steeply dipping NE-SW to ENE-WSW striking fault zone. Piezometric heads remained consistently 2 to 3 m below the ground surface (mgbs) throughout the tested depth interval (35 to 240 mbgs), indicating strong hydraulic connectivity within the fault zone and the absence of a significant vertical head gradient. The Ban-1 borehole was tested below the steel-cased section at 200 mbgs in six intervals of variable length and depth. Packer placement was limited to the zone of intact claystone between 200 mbgs and 230 mbgs. Tests for intervals between a single-packer and the bottom of the hole facilitated tests over a larger depth range. Various pulse, slug, and constant flow rate injection tests were applied. The results show hydraulic conductivities between 2×10^{-10} m/s and 8×10^{-9} m/s. The piezometric head was measured before the test program at a depth of 56 mbgs. Hydrogeological tests for 150 mbgs in the Aub-1 borehole show comparably high hydraulic conductivities as in the Cot-1 borehole, with values ranging between 2×10^{-5} m/s and 3×10^{-8} m/s. Constant piezometric heads were measured between 8 and 9 mbgs.

The piezometric heads measured in the wells in S-Limburg and along the Soumagne trajectory show a groundwater surface that mostly follows the topography within a 100–150 m distance in the hillier S and a few meters to a few decameters in the shallower N.

Geotechnical conditions

The results of a total of 20 uniaxial compressive strength tests and 40 Brazilian tensile strength tests on samples from all the outcrops are presented in Fig. 14; Table 3. Mean UCS values range between 107 MPa for Viséan limestones from Richelle and 373 MPa for quartzitic, Namurian sandstones from Plombières. BTS mean values range from a minimum of 6 MPa for Frasnian limestone to a maximum of 29 MPa for the sandstone. Laboratory investigations on the core material from Aub-1 and Cot-1 comprise 28 UCS and 38 BTS tests on sandstone and siltstone samples. Sandstone samples from the Aub-1 borehole exhibited uniaxial compressive strengths ranging from 114 to 266 MPa, with a mean of 172 MPa. The siltstone possessed a mean strength of 95 MPa with values between 42 MPa and 134 MPa. BTS tests gave a range of values between 11 MPa and 22 MPa with a mean of 16 MPa for sandstone samples. Siltstones were tested with results between 6 MPa and 21 MPa and a mean of 12 MPa. 15 sandstone and siltstone samples from various depths of the Cot-1 borehole were tested. UCS values for nine tested siltstone samples range between 35 MPa and 155 MPa, with a mean of 72 MPa. Six sandstone

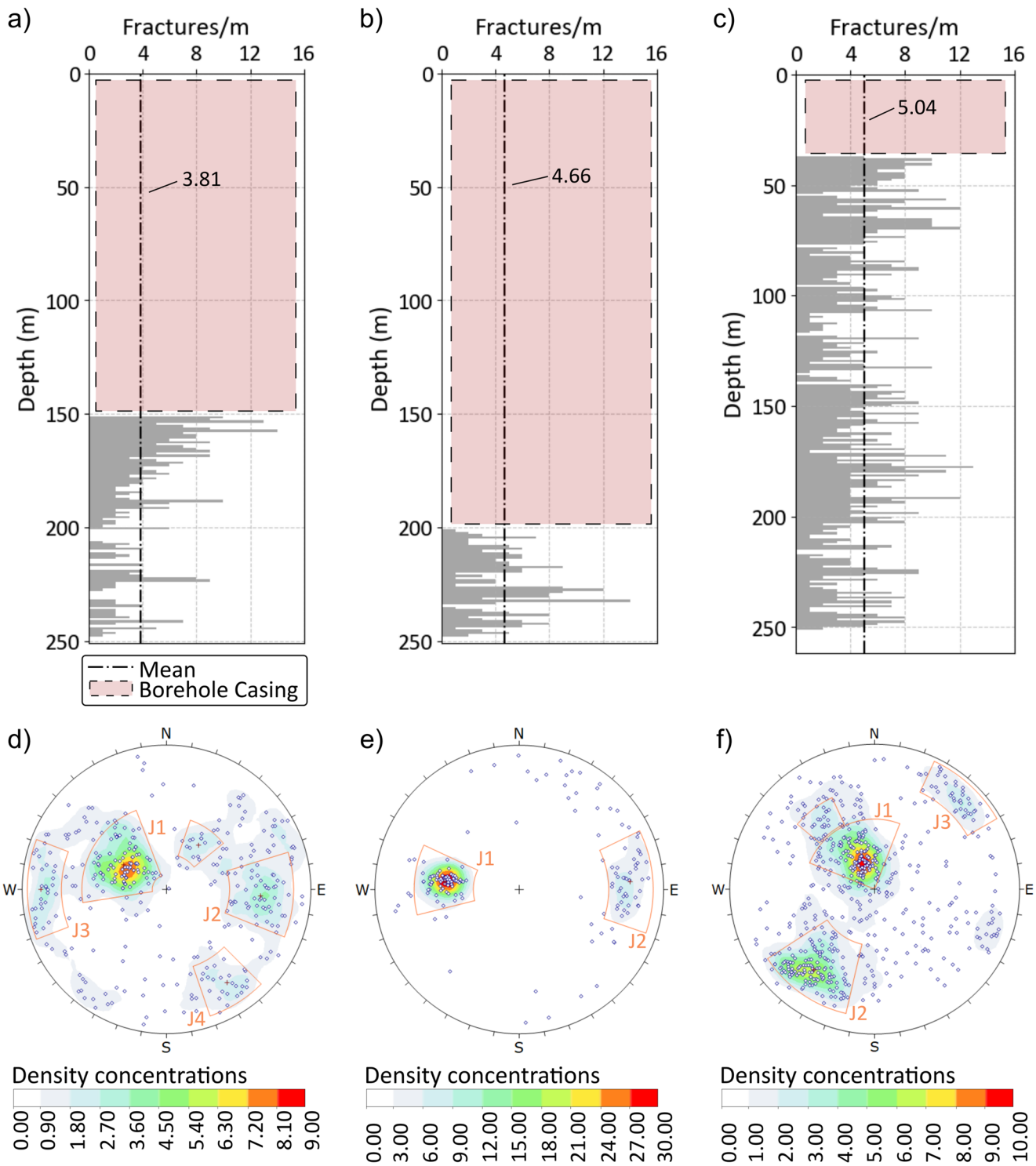

Fig. 12 Discontinuity characteristics of the boreholes: **a**), **b**), and **c**) show fracture densities plotted against the borehole depth per metre for Aub-1, Ban-1, and Cot-1, respectively. Additionally, the mean fracture density is indicated for each borehole. Lower hemisphere stereo projections of discontinuities for the respective boreholes are given in **d**), **e**), and **f**). The dominant fracture set JN1 is assumed to be bedding-parallel for all boreholes

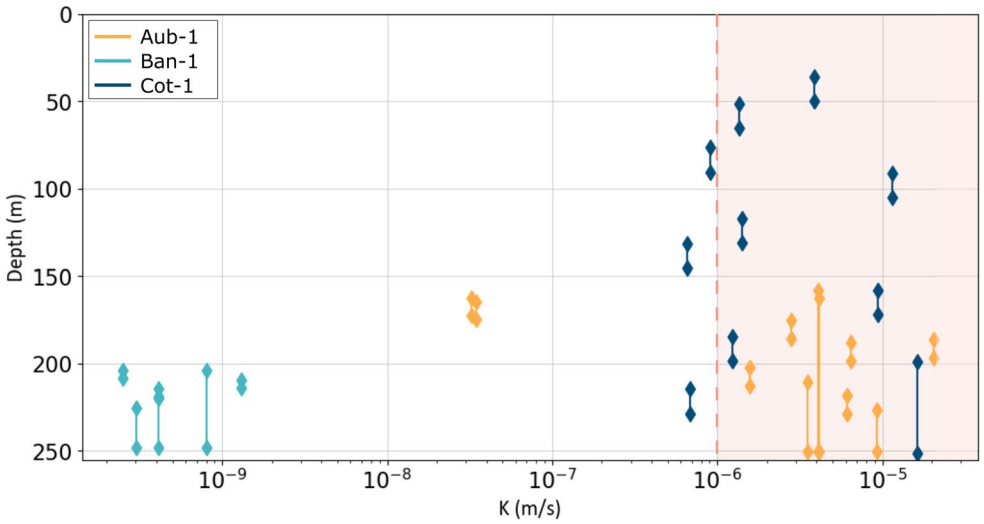

Fig. 13 Distribution of hydraulic conductivities in the Aub-1, Ban-1 and Cot-1 boreholes plotted against borehole depth. Hydraulic conductivities higher than 10^{-6} m/s (red dashed line) are supposed to result in significant water flow to the subsurface infrastructures

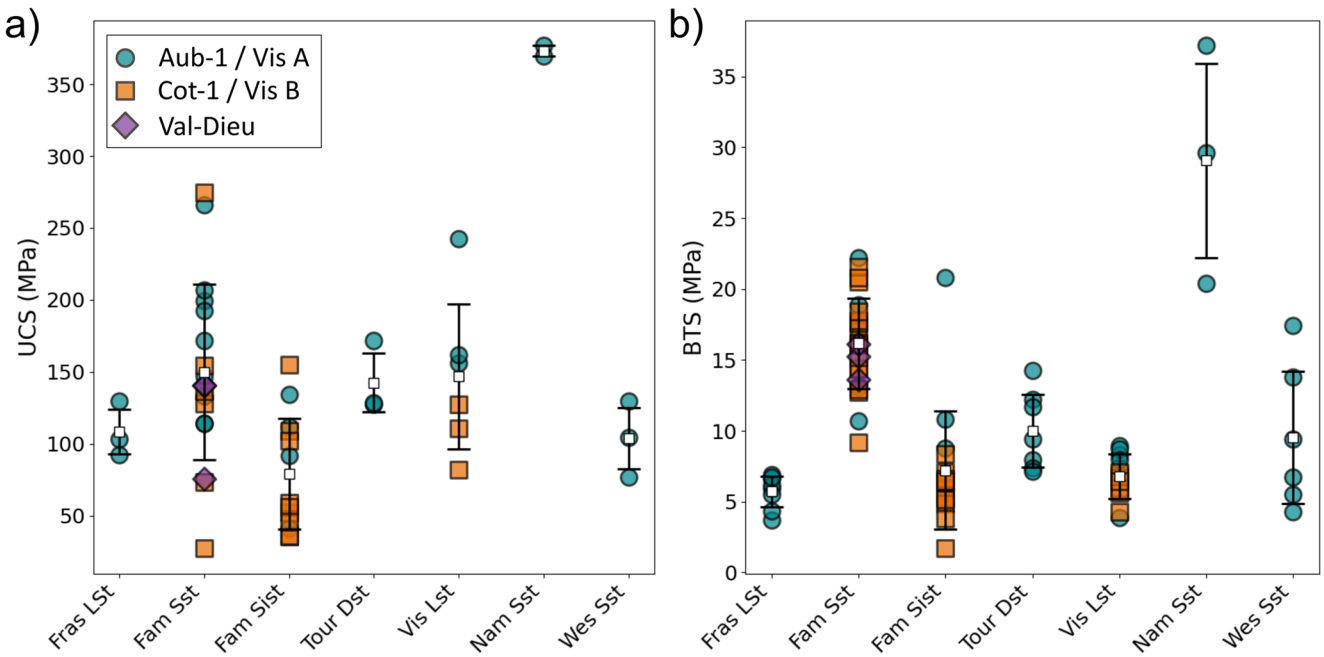

Fig. 14 Results of (**a**) UCS and (**b**) BTS tests on samples from Aub-1, Cot-1 and outcrops. Fras = Frasnian, Fam = Famennian, Tour = Tournaisian, Vis = Viséan, Nam = Namurian, Wes = Westphalian, SisT = Siltstone, Sst = Sandstone, Lst = Limestone, Dst = Dolostone. Vis A refers to the Viséan limestone samples from the Carnol quarry, Vis B to those from Richelle. Val-Dieu indicates the Famennian sandstone samples from the road-cut in Val-Dieu

samples from Cot-1 showed a uniaxial compressive strength between 27 MPa and 275 MPa with a mean UCS of 132 MPa. BTS values were determined on a total of 24 samples where nine siltstone samples had values of between 4 MPa and 8 MPa, with a mean of 6 MPa, while sandstone samples ranged between 9 MPa and 22 MPa with a mean of 16 MPa.

Most lithologies display characteristic ranges in both tensile and compressive strength. Lower strength values were frequently associated with shear failure along pre-existing planes of weakness, such as joints and fractures (Fig. 15a), resulting in notable reductions in peak strength compared to intact rock samples. Additionally, samples exhibiting signs of weathering, such as discoloration, as observed in the Westphalian sandstones from the Wurm Valley outcrop, also demonstrated reduced strength (Fig. 15c). Figure 15b/d show samples of Condroz Sandstone and Westphalian sandstone, respectively which showed the maximum UCS.

Cerchar Abrasivity Index tests (CAI) were conducted on cut and broken surfaced Famennian samples from the Cot-1 borehole and on samples from outcrops (Fig. 16). The results varied between 0.28 and 5.75, representing extremely low to extremely high values. In particular, the Famennian

Table 3 Summary of UCS and BTS test results on samples from outcrops, Aub-1, and Cot-1 boreholes. Fras = Frasnian, Fam = Famennian, Tour = Tournaisian, Vis = Viséan, Nam = Namurian, Wes = Westphalian, SisT = Siltstone, Sst = Sandstone, Lst = Limestone, Dst = Dolostone. Vis Lst A refers to the viséan limestone samples from the carnol quarry, Vis Lst B to those from Richelle

Stratigraphic unit	Sample ref.	UCS [MPa]				BTS [MPa]			
		Min.	Max.	Mean ± SD	Nb.	Min.	Max.	Mean ± SD	Nb.
Westphalian	Wes Sst	77	130	104 ± *22*	3	4.3	17.4	9.5 ± *4.7*	6
Namurian	Nam Sst	370	377	373 ± *4*	2	20.4	37.2	29.1 ± *6.9*	3
Viséan	Vis Lst A	156	242	186 ± *39*	3	3.9	9.0	*7.5 ± 1.7*	6
Viséan	Vis Lst B	82	127	*106 ± 19*	3	4.3	7.1	6.0 ± *0.9*	6
Tornaisian	Tour Dst	128	172	143 ± *21*	3	7.1	14.3	10.0 ± *2.5*	7
Famennian	Fam Sst	76	141	119 ± *31*	3	13.6	16.1	15.0 ± *1.0*	3
Famennian	Aub-1 Sst	114	266	*172 ± 47*	9	10.7	22.2	*16.3 ± 3.5*	8
Famennian	Aub-1 Sist	42	134	*95 ± 34*	4	5.6	20.8	*11.5 ± 5.7*	4
Famennian	Cot-1 Sst	27	275	133 ± *77*	6	9.2	21.5	*16.3 ± 3.2*	15
Famennian	Cot-1 Sist	35	155	72 ± *39*	9	1.7	8.3	*5.7 ± 1.7*	11
Frasnian	Fras Lst	93	130	109 ± *16*	3	3.7	6.9	5.7 ± *1.1*	8

Sandstone exhibited high abrasiveness. Viséan limestone from both investigated outcrops possessed the lowest abrasiveness, ranging from extremely low to low CAI. Siltstone samples from the Cot-1 borehole also possessed extremely low abrasiveness, but a wider range, with CAI values in the medium category. Famennian sandstone from the investigated road cut and the Cot-1 borehole showed very high abrasiveness. The borehole samples exhibit a wide range, from low to extremely low, with a mean CAI value that can be categorized as very high.

Regional stress conditions

In situ stress data from the area of interest are limited, especially regarding stress magnitudes. Regional stress data from shallow to intermediate depths, as needed for planning ET infrastructure, are absent. Nevertheless, various authors report a general SE-NW directed maximum horizontal stress (SH) for Central Europe (Müller et al. 1992; Heidbach et al. 2018; Morawietz et al. 2020; Ahlers et al. 2021a). The data presented in Fig. 17 from the World Stress Map project (WSM) for the area are mainly based on earthquake focal mechanisms (Trautwein-Bruns et al. 2010; Reiter et al. 2016). A recent crustal 3D stress state model for Germany encompasses the current area of investigation and substantially supports the aforementioned trend of a SE-NW directed trend for S_H (Ahlers et al. 2021b). The same applies to borehole breakout-based in-situ stress analyses carried out by Trautwein-Bruns et al. (2010) within the RWTH-1 well in Aachen, where quoted minimum and maximum horizontal stress gradients were 0.019 MPa/m and 0.038 MPa/m, respectively.

Hydraulic Fracturing (HF) and Hydraulic testing of pre-existing fractures (HTPF) were conducted in the Cot-1 borehole to estimate the in-situ stress conditions at shallow to intermediate depths. However, the fracture density within the Cot-1 borehole limited the packer and interval positions for the tests. High hydraulic conductivities further restrained the tests. Tests at five intervals for depths of 66.2, 116.8, 127.3, 135.8, and 221.7 mbgs were performed. The testing did not reveal a distinct fracture initiation. Tests at 66.2, 116.8, 127.3, and 135.8 mbgs entailed hydraulic stimulation of pre-existing fractures without distinct breakout events. The limitations of the dataset prevent the derivation of the principal horizontal stress components. However, normal stresses (σ_n) on stimulated fracture planes show a depth-dependent increase from 1.3 MPa to 2 MPa between 66 m and 135.8 mbgs. In the test section at 221.7 m, the high hydraulic conductivity prevents a reliable derivation of σ_n. The vertical stress component (σ_v) was calculated with an assumed rock mass density of 2.5 g/cm^3. The vertical and normal stresses evaluated from the measurements are presented in Table 4, expressed in terms of test depth.

Probabilistic ground behavior

The Austrian Society of Geomechanics defines the ground type as a homogenous rock mass in terms of parameters such as rock type, rock strength and deformational behavior, the discontinuity network and properties, and hydraulic properties. Hence, different ground types exhibit varying characteristics that influence their behavior (ÖGG 2021). The ground behavior type (BT) refers to the response of the rock mass to the excavation of the entire cross-section, considering the ground type(s) but without considering sequential excavation and support measures (Solak 2009; ÖGG 2021). The general ground behavior types defined by ÖGG (2021) are shown in Table 5.

Probabilistic ground behavior predictions for a potential ET layout with tunnels connecting the boreholes Aub-1, Ban-1, and Cot-1 were established. Geological, geotechnical, and hydrogeological data from this study served as

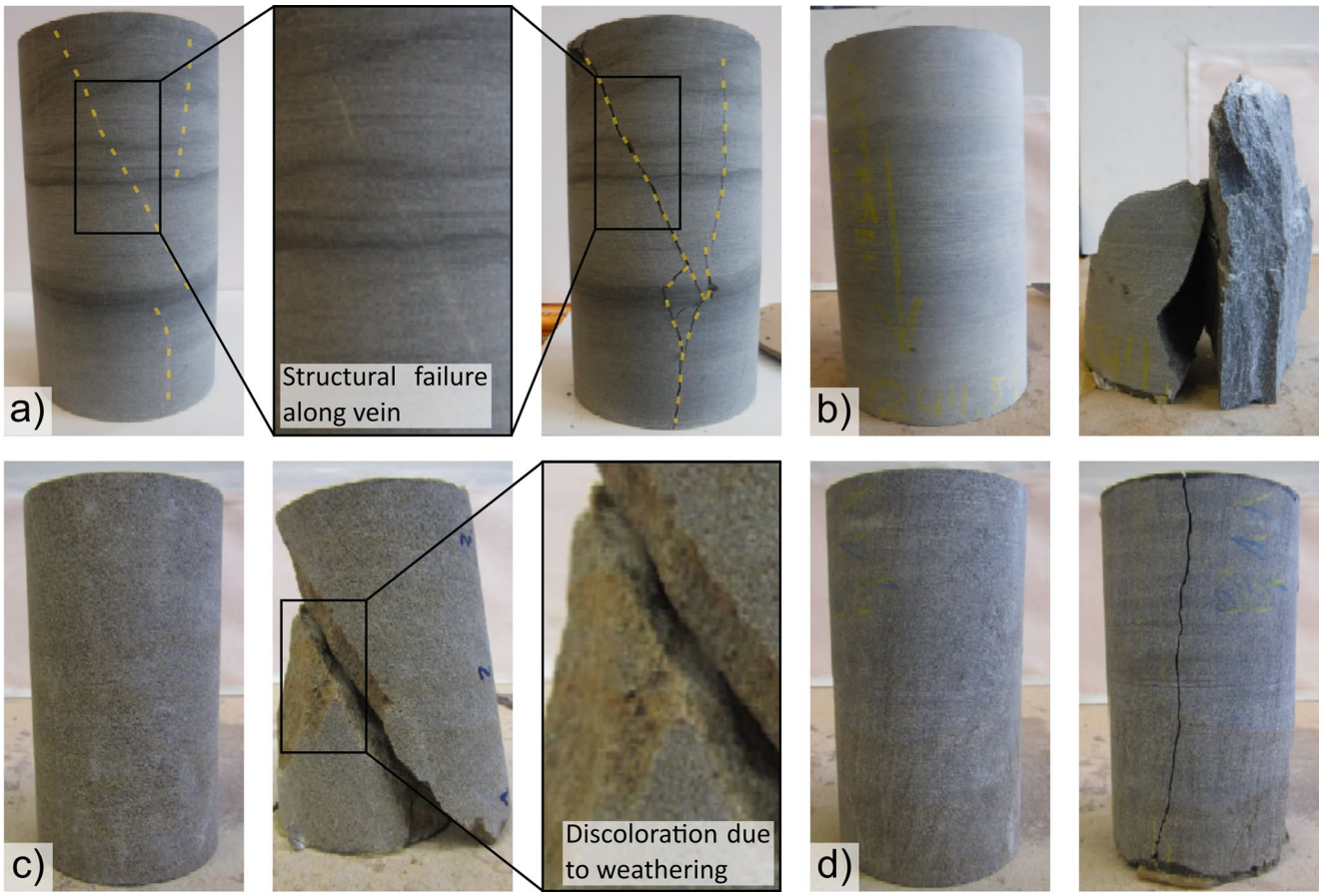

Fig. 15 Examples of uniaxial compressive strength (UCS) samples of Condroz Sandstone from Cot-1 (a/b) and from the Wurm valley outcrop (c/d). Samples a and c showed the minimum and b and d the maximum strength values for their respective lithologies. (**a**) Structural failure along recrystallized veins led to a greatly reduced peak strength compared with other samples of the same lithology, (**b**) Condroz sandstone sample from Cot-1 with the highest measured UCS value for this lithology, (**c**) Sandstone sample from the Wurm valley outcrop that showed brownish discoloration due to weathering, resulting in the lowest measured UCS of this lithology and (**d**) Grey unweathered sample of sandstone from the Wurm valley outcrop that showed the highest measured UCS of this lithology

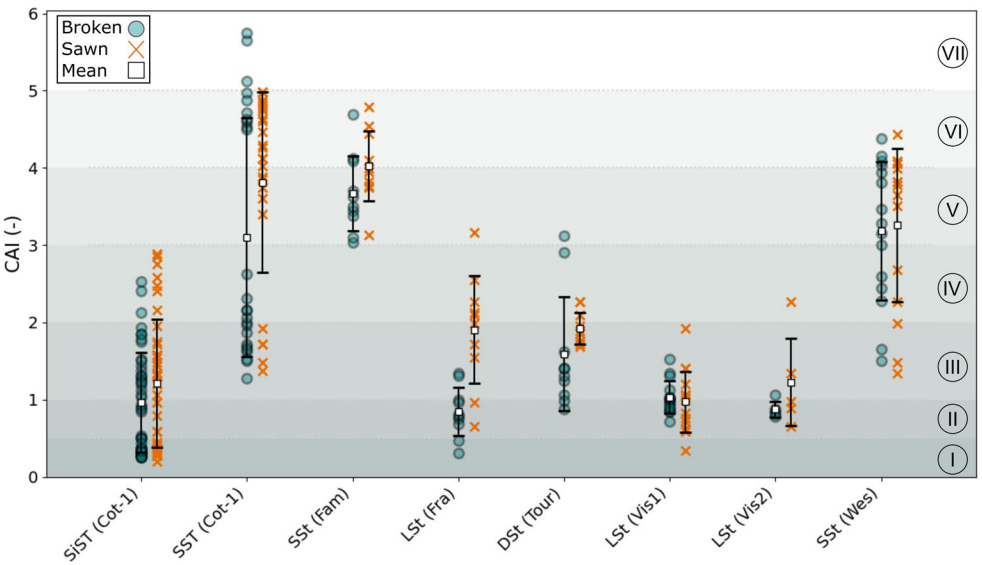

Fig. 16 Results of the Cerchar abrasivity tests on broken and sawn sample surfaces from Cot-1 and outcrops. Abrasivity categories according to the standard of the German Society of Geotechnics are indicated with Roman letters: **I** = extremely low, **II** = very low, **III** = low, **IV** = medium, **V** = high, **VI** = very high, **VII** = extremely high

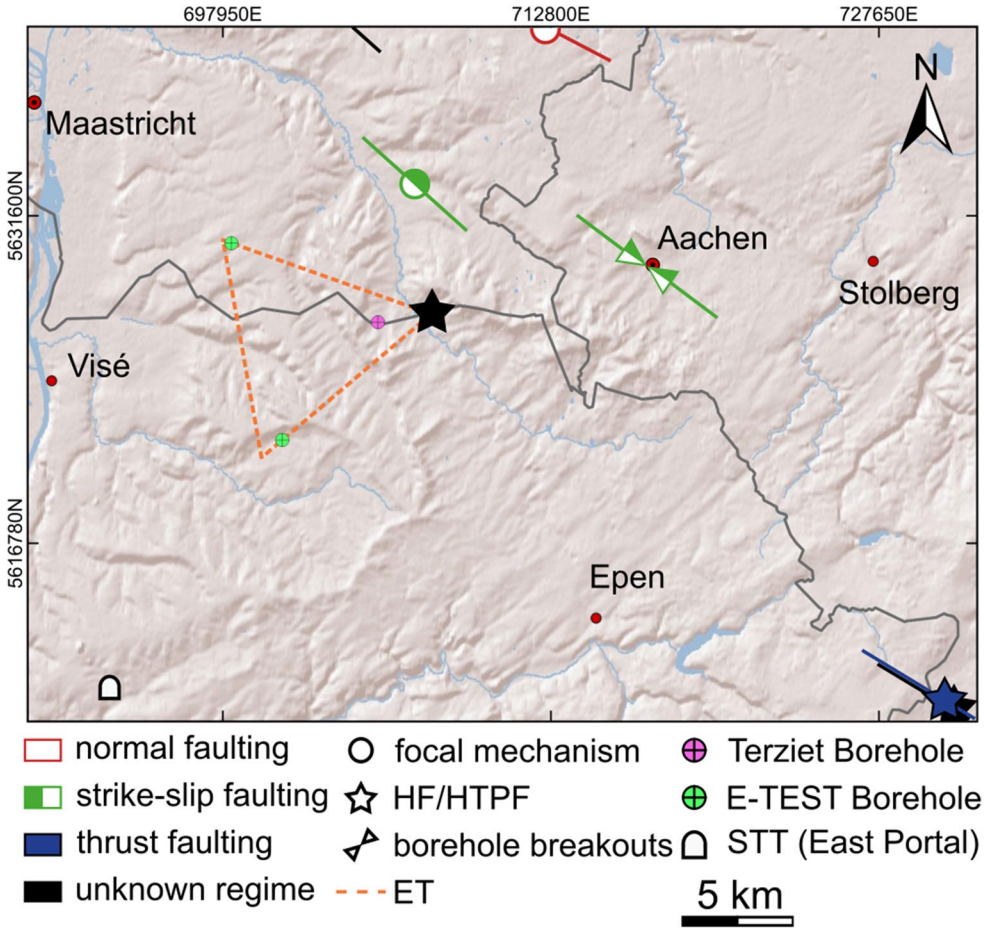

Fig. 17 Stress conditions within the investigation area. Regional stress trends taken from the WSM (Reiter et al. 2016) with an indication of the methods used. The marker-lines indicate the general stress direction of maximum horizontal stress

Table 4 Results of the hydraulic stress measurements within the Cot-1 borehole. σ_v = vertical stress component, σ_n = normal stress on stimulated fracture plane, HTPF = Hydraulic testing of pre-existing fractures

Depth [mbgs]	σ_v [MPa]	σ_n [MPa]	Test type
66.2	1.6	1.3	HTPF
116.8	2.9	1.8	HTPF
127.3	3.1	2	HTPF
135.8	3.3	2	HTPF
221.7	5.4	x	Step rate test

input for defining the individual ground types. The geological sequences likely to be penetrated by the individual tunnels were sampled at 10-m intervals from an unpublished geological model of the region (Chudalla et al., in prep.). At this stage of the project, major uncertainty remains, with knowledge-based uncertainty (epistemic uncertainty) prevailing, as different geological scenarios with strongly contrasting structural implications exist. Furthermore, stochastic uncertainty is inherently included in the available input data (Wellmann et al. 2010). As more knowledge about the subsurface is gained, both sources of uncertainty will be reduced, but not eliminated; therefore, the ongoing work needs to maintain careful tracking and modeling of uncertainties. Given the current state of data availability, the authors consequently chose a less complex and more generalizable model. For the same reason, the fault zones are assumed to have one of only two possible dip angles. The authors acknowledge that this model does not fully encapsulate the complexity of the expected ground conditions; new information can be used to update both the structural geological model and the geotechnical model based on it. Furthermore, uncertainty estimates based on model input can be obtained by automatically computing different 3D model realizations and using Monte Carlo simulations (Wellmann et al. 2010). In this approach, the probabilities of the occurrence of each stratigraphy at a particular point can be specified. This workflow is applicable even for structurally complex models (see Brisson et al. 2023); however, it is beyond the scope of this study and will be published separately.

The ground types for the ground behavior model were defined based on lithological and stratigraphic boundaries, as well as geotechnical properties. Mean intact rock properties were derived from the laboratory investigation of this study (σ_c, σ_t, ν, E, γ). The Hoek-Brown constant values (m_i) were estimated based on Hoek (2007). Where available, the

Table 5 General categories of ground behavior types and potential resulting failure modes (from ÖGG, 2021)

Behavior Type (BT)		Description of potential failure modes/mechanisms during excavation of the unsupported rock mass
1	Stable	Stable rock mass with the potential of small local gravity-induced falling or sliding of blocks
2	Discontinuity-controlled block failure	Deep-reaching, discontinuity-controlled, gravity-induced falling and sliding of blocks, and occasional local shear failure occur
3	Shallow stress-induced failure	Shallow stress-induced brittle and shear failures in combination with discontinuity and gravity-controlled failure of the rock mass
4	Deep-seated stress-induced failure	Deep-seated stress-induced brittle and shear failures in combination with large displacements
5	Rock burst	Sudden and violent failure of the rock mass, caused by highly stressed brittle rocks and the rapid release of accumulated strain energy
6	Buckling failure	Buckling of rocks with a narrowly spaced discontinuity set, frequently associated with shear failure
7	Shear failure under low confining pressure	Potential for excessive overbreak and progressive shear failure with the development of chimney type failure, caused mainly by a deficiency of side pressure
8	Ravelling ground	Flow of cohesionless dry or moist, intensely fractured rocks or soil
9	Flowing ground	Flow of intensely fractured rocks or soil with high water content
10	Swelling	Time-dependent volume increase of the rock mass caused by physical-chemical reaction of rock and water in combination with stress relief, leading to inward movement of the tunnel perimeter
11	Frequently changing behavior	Rapid variations of stresses and deformations caused by heterogeneous rock mass conditions or block-in-matrix rock situations of a tectonic melange (brittle fault zone)

borehole-derived geotechnical data (Famennian rocks) were used. GSI values were derived from the well-known characterization chart for blocky rock masses first introduced by Hoek (1994) and extended by Marinos and Hoek (2000). The friction angle (φ) and rock matrix cohesion (c) were calculated using the Mohr-Coulomb criterion, as described by Hoek et al. (2002). A conservative approach was chosen for geotechnical input parameters, assuming the lowest geotechnical properties for each stratigraphic unit. Spatial fracture orientations were implemented based on the structural evaluations from outcrops and boreholes. Major fault zones (on the km scale and visible on the map) were characterized in terms of the fault damage zone (FDZ) and the presence of fault gouge (FG). Fault zone geometries (dip-angle and displacement) were derived from (Cambier and Dejonghe 2010, 2012) and projected from the surface to the tunnel line. For simplification, Variscan thrust faults were modeled with a general dip angle of 50°, whereas for the younger NW-SE striking normal faults, it was assumed that they were subvertical (Cambier and Dejonghe 2010, 2012). Major thrust faults in the vicinity of the proposed ET layout, such as the Morsenet fault, exhibited displacements of up to 1,000 m. However, the displacements reported by Cambier and Dejonghe (2010, 2012) spanned a wide range, from 10 m to several kilometres. FDZ and FG thicknesses were estimated at 100 m and 10 m, respectively, based on the correlations between fault displacement and FDZ/FG thickness reported by Torabi et al. (2019) and Torabi and Berg (2011) for siliciclastic rock, with an assumed displacement of 250 m.

Table 6 presents the different geotechnical intervals from the present study, where bold-italic lettering indicates the geotechnical intervals considered for the ground behavior modeling approach. The Devonian rock masses are represented by the investigated siltstone units from the Cot-1 borehole, and the Carboniferous rock masses are composed of Westphalian sandstone. Figure 18 shows the tunnel alignment for each tunnel section, the actual interpretation of the geological unit, and the resulting ground behavior types.

Regarding the current status of the geological model and the proposed tunnel alignment, the ET tunnels would predominantly penetrate Upper Devonian rock masses. Non-faulted Devonian rock sequences show ground behavior type one, corresponding to stable ground conditions. Tunnel sequences penetrating Upper Carboniferous rock units are characterized by ground behavior types of class two, representing the potential of discontinuity-controlled block and wedge failure. Fault zones show a combination of the ground behavior types four, eight, and eleven. In general, the ground behavior modeling results give a first idea of the response of the subsurface to excavation processes and emphasize (a) the necessity of block and wedge support for sections of the ET tunnels and (b) unstable ground conditions in the vicinity of fault zones, and especially in caverns.

Implications for the Einstein telescope

Identifying a suitable site for constructing and operating the third-generation gravitational-wave observatory, the "Einstein Telescope," involves a complex set of criteria. In contrast to conventional underground infrastructure, such as traffic tunnels or gas and oil storage facilities, additional constraints must be considered, primarily governed by the demand for a quiet subsurface environment, particularly regarding ambient noise. Proximity to sources of anthropogenic noise must therefore be avoided. At the same time, soft geological units provide attenuating characteristics, which benefit undisturbed ET performance. Additionally,

Table 6 Defined ground types from this study and their mean intact rock properties required for the ground behavior prediction. Chosen geotechnical units as data input for the ground behavior model are indicated by bold-italic lettering. σ_c = Uniaxial compressive strength, σ_t,= Brazilian tensile strength ν = Poisson´s ratio, E = Modulus of elasticity, γ = specific weight, UD = Upper Devonian, LC = Lower Carboniferous, C = Carboniferous (undivided), FDZ = Fault damage Zone, FG = Fault gouge

Geotechnical Unit	σ_c (MPa)	m_i (-)	GSI (-)	ν (-)	E (GPa)	γ (kN/m^3)	σ_t (MPa)	φ(°)	c (MPa)	Group
Westphalian Sandstone	***104***	***15***	***55***	***0.25***	***20***	***23***	***10***	***35.5***	***6.3***	C
Namurian Sandstone	373	17	70	0.25	31	25	29	41.0	29.5	
Viséan Limestone	147	10	65	0.25	27	26	7	34.9	9.5	
Tournaisian Dolostone	143	10	65	0.25	27	27	10	34.9	9.2	
Famennian Siltstone	***72***	***7***	***65***	***0.25***	***11***	***26***	***12***	***31.8***	***4.3***	UD
Famennian Sandstone	133	17	65	0.25	28	26	15	39.6	9.7	
Frasnian Limestone	109	9	55	0.25	24	23	6	31.1	5.7	
FDZ	***2***	***4***	***25***	***0.30***	***15***	***25***	***0.5***	***25.2***	***1.7***	FDZ
FG	***1***	***2***	***18***	***0.30***	***10***	***25***	***0.1***	***22.6***	***0.03***	FG

environmental noise considerations, geological, geotechnical, and hydrogeological conditions will dictate the feasibility of excavation methods, the design of rock support systems, and the implementation of grouting and drainage strategies. The investigations presented in this study address key aspects of siting and feasibility assessment, aiming to provide a foundation for more detailed site characterization in the Euregio Meuse-Rhine (EMR) region. The results of these investigations are discussed below with a focus on their implications for future siting decisions.

Subsurface conditions and geological constraints

Geological investigations in the EMR reveal a heterogeneous subsurface characterized by variable and diverse sedimentary lithologies, as well as a strong tectonic overprint resulting from Variscan compression and Mesozoic to recent rift tectonics associated with the Lower Rhine Graben. Several discontinuity sets with various spatial orientations have been identified in outcrops and boreholes. Discontinuities with predominant SW-NE strike, observed in the Carnol quarry (BE), the sandstone outcrop within the Wurm valley (Ger), and boreholes Cot-1 and Aub-1 are likely associated with Variscan compressional deformation. In contrast, a prominent NW–SE striking set, seen in Cot-1, as well as in the Val-Dieu road cut and Wurm valley outcrop, aligns with the orientation of normal fault systems related to the Lower Rhine Graben. Similar orientations (SW–NE and NW–SE) were also described by Trautwein-Bruns et al. (2010, 2011) based on geophysical well logs from the RWTH-1 borehole in Aachen. Additional discontinuity sets, particularly with NNE–SSW trends identified in the Aub-1 and Ban-1 boreholes, cannot be clearly attributed to a single tectonic event, highlighting the challenge of extrapolating discontinuity data from localized investigations to a broader regional context. Consequently, SW–NE and NW–SE trending discontinuities are expected throughout the region. Depending on the orientation of underground structures, these may lead to structurally controlled failure mechanisms, such as sliding along planar surfaces, or block and wedge instability. The presence of multiple, locally variable discontinuity sets could further exacerbate instability risks, especially within cavern excavations. A detailed structural analysis of the discontinuity network at each proposed ET vertex is therefore essential to mitigate risks related to structurally controlled failures.

Hydrogeological observations indicate that fractured zones in both Cot-1 and Aub-1 exhibit elevated hydraulic conductivities, suggesting significant potential for groundwater inflow during tunnel and cavern construction. The measured conductivities range over several orders of magnitude, making it difficult to predict the quantification of potential water inflows into excavations and the requirements for pumping to safely manage these. Moreover, fault zones and potentially karstified formations will need to be traversed, resulting in abrupt changes in hydrogeological conditions and significant variations in water inflow. Such zones may require extensive grouting works before, during, and after construction works to reduce water inflows. Accordingly, a robust water management strategy must be developed, based on a detailed hydrogeological model. This is particularly important at ET vertex locations, where cavern excavations are planned, as natural groundwater flow can induce gravity-gradient noise (Akutsu et al. 2018).

The Upper Devonian Condroz Sandstone Group appears to offer favorable geological conditions for hosting caverns, owing to its considerable thickness of competent section with high intact rock strength. Laboratory tests on samples from two boreholes (Aub-1 and Cot-1) and one outcrop (Val-Dieu) confirmed high uniaxial compressive and tensile strengths, supporting its suitability and favorable conditions for excavation activities.

However, the rock mass quality, as indicated by RQD values, varied significantly between the boreholes. While

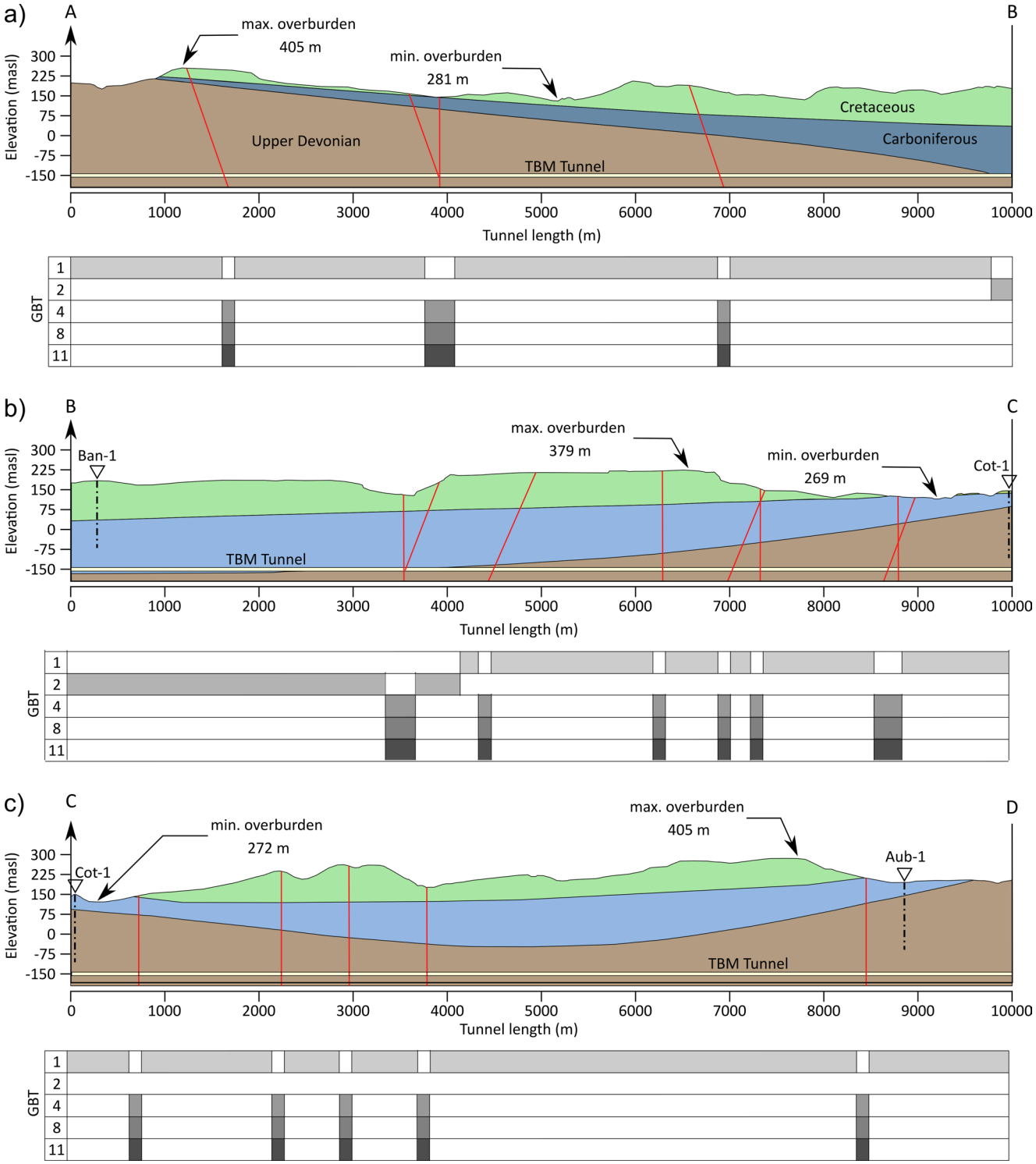

Fig. 18 Results of the ground behavior modelling for a potential ET tunnel layout. The respective sections roughly connect the boreholes (**a**) Aub-1 with Ban-1, (**b**) Ban-1 with Cot-1 and, (**c**) Cot-1 with Aub-1. The borehole positions are indicated for the cross-sections b) and c), where the proposed tunnel layout cuts the respective locations. Red lines symbolize fault zones projected from the surface to the tunnel trajectory at a depth of 150 m below sea level. The minimum and maximum values of tunnel overburden are specified for each cross-section. The ground behavior types (GBT) are indicated along the individual tunnel trajectories

core material from Aub-1 generally indicated good rock mass conditions, samples from Cot-1 were predominantly of poor quality. The Cot-1 borehole is situated close to several fault zones, whereas no major fault structures have been identified in the vicinity of Aub-1. This discrepancy suggests a strong tectonic overprint on the rock mass quality of the Condroz Sandstone Group sequences, despite otherwise favorable rock properties. This tectonic overprint may also significantly influence potential groundwater inflow, as fault-related fracturing can create preferential flow paths, potentially increasing inflow rates by several orders of magnitude in the vicinity of fault zones.

Lower Carboniferous units exhibit high intact rock strength, but the potential presence of karst features constrains their suitability for cavern development. Among the tested formations, Namurian sandstones demonstrated the highest tensile and compressive strengths. However, they are typically interbedded with weaker shale and siltstone units, and may be associated with coal-bearing strata, all of which can impose additional challenges for excavation and support. Notably, both Carboniferous units in this study were evaluated exclusively through outcrop data. Their spatial extent, as well as their geotechnical and hydrogeological properties at depth, requires further subsurface investigation.

The in-situ stress (HTPF) measurements in the Cot-1 borehole could not define the local stress conditions in terms of principal horizontal stress magnitudes and orientations. However, under the assumption that the stimulated fractures are oriented perpendicular to one of the principal horizontal stresses, σ_h (minimum horizontal stress) and σ_H (maximum horizontal stress), the ratio of horizontal to vertical stress (k) would imply two possibilities:

i. $k_{min} < 1 < k_{max}$ corresponding to a strike-slip faulting regime;
ii. $k_{min} < k_{max} < 1$ corresponding to a normal faulting regime.

Since k_{min} is less than one, it is concluded that the system is not under a compressive (thrust faulting) stress regime, and residual tectonic stresses down to the target depth of 250 m appear to be low. Given the rock strengths observed during the geotechnical investigations of this study, stress-induced failure of non-faulted Paleozoic rock sequences is unlikely to occur. However, problematic conditions may arise in the soft shale sequences of the Namurian, where decomposition due to swelling clay minerals needs to be taken into account. The low strength may lead to squeezing ground conditions, necessitating careful consideration in planning appropriate stabilization and excavation support measures.

Considerations for excavation and support design

The excavation and support strategies proposed here are based on an early-stage site characterization and remain preliminary. Due to the limited availability of subsurface data at the target depth of the Einstein Telescope and the high geological complexity of the study area, the current modeling is coarse and constrained by significant uncertainty. The geological framework is strongly influenced by multiple tectonic events, including Variscan compression and extensional faulting related to the Lower Rhine Graben, resulting in spatially variable lithologies, discontinuity patterns, and hydrogeological conditions. The anticipated variability in ground behavior, particularly in structurally complex or faulted zones, underscores the necessity of a flexible, observational tunneling approach combined with real-time monitoring and advance probing.

The large cavern structures should ideally be placed in homogeneous, competent, and thick rock mass sections. However, large excavations are prone to structurally controlled instabilities, such as rock wedge failure, which require heavy rock support, i.e., achieved with long and heavy rock bolts and anchors, as well as thick reinforced concrete lining (Singh and Goel 2011; Amann et al. 2022). A site-specific cavern layout and support design at each ET vertex, with cavern orientation, shape, and size adapted to the geological and, in particular, structural conditions, could help mitigate block and wedge formation. Additionally, vaulted cavern shapes may further reduce local stress concentrations, thereby limiting the risk of stress-induced instabilities (Amann et al. 2022).

The tunnels are likely to penetrate variable geological conditions. In non-faulted rock mass sections where stable ground conditions (ground behavior type 1) can be expected, such as expectably competent sections of the Condroz Sandstone Group, full-face excavation with mechanical excavation methods and minimal support is expected to be sufficient. Local reinforcement in areas prone to small-scale wedge and block detachment might be required and could be achievable with spot bolting and occasional shotcrete application. Where long and continuous tunnel drives are feasible, the use of Tunnel Boring Machines (TBM) could be applicable and efficient. However, their successful deployment requires a predictable geological environment that is currently not confirmed. In contrast, sequential excavation methods may provide greater flexibility in heterogeneous ground conditions, where rapid geological changes could interrupt continuous TBM operation, potentially leading to trapped machines and high associated costs (Goel 2016; Gong et al. 2016).

The ground behavior modelling indicated a high likelihood of increased block and wedge failure for Carboniferous

tunnel sections. Sequential excavation with systematic rock bolting, along with fibre reinforced shotcrete, would help mitigate potential structural instabilities. Special and fast-adaptable excavation and support methods will be needed when fault zones are encountered during tunneling processes.

More extensive and complex support and reinforcement measures are required in heterogeneous tunnel sections, such as heavily fractured zones, karst features, weak materials (e.g., shale, unconsolidated clay, coal seams), or faulted ground, where poor rock mass quality leads to reduced stand-up time after excavation (Bieniawski 1989). These zones will require immediate and robust support installation, including the use of reinforced shotcrete, steel-mesh or ribs as well as anchors or rock bolts. Additional measures in especially weak zones can include forepoling systems or canopy tubes installed as pre-support in the tunnel crown, pre-grouting strategies ahead of the tunnel face, and potentially backfill methods, especially in the potentially karst-bearing Lower Carboniferous formations (Cheng et al. 2017; Li et al. 2021; Tacim et al. 2023). Moreover, as previously indicated, significant groundwater inflow may necessitate additional measures for hydraulic and structural stabilization. Pre-excavation grouting represents a viable option to reduce water ingress and, simultaneously, to enhance the self-supporting capacity of the surrounding rock mass, thereby contributing to the overall effectiveness and durability of the tunnel support system.

Considering these factors, a mechanical excavation approach with the capacity for both continuous and cyclic advance could be most appropriate in early design phases. This should be paired with a robust observational method, including constant monitoring, advance probing, and the capacity to rapidly adjust excavation techniques and support schemes in response to encountered conditions. Such an approach is embodied in the New Austrian Tunneling Method (NATM), which emphasizes real-time feedback, staged support installation with the possibility to adapt to changing conditions, and optimization of ground-structure interaction (Hemphill 2012). A successful implementation of this approach was achieved in the Soumagne train tunnel, located partly on the southwestern margin of the study area, where adaptable excavation and support strategies enabled efficient tunneling through variable and complex Viséan, Namurian, and Westphalian lithologies (Janssens et al. 2005).

However, the technical and economic feasibility of this approach requires further investigation, particularly in view of the total combined length of all three tunnel sections, including rock mechanical assessments and subsequent dimensioning, achievable through a combination of empirical methods (e.g., RMR, Q-System, GSI), analytical methods, and numerical methods.

Conclusion and outlook

The construction feasibility, as well as the scientific performance and measurement-reliability of the Einstein Telescope (ET), are closely tied to several site requirements, governed by the demand for low ambient noise and favorable geological conditions that provide attenuating benefits through soft, unconsolidated strata on the top of thick and hard rock sequences, constituting the potential host formations for tunnel and cavern facilities. The preliminary site exploration of the Euregio-Meuse-Rhine (EMR) area, one of the currently considered sites for the ET, has provided insights into important site characteristics with a focus on geological base criteria. The positioning of the ET in the EMR should prioritize the avoidance of anthropogenic noise sources, including wind turbines, major roads, and railway lines, which can significantly impair detector sensitivity. Where complete avoidance is not feasible, the presence of an overburden of soft sedimentary units, particularly Cretaceous and Cenozoic formations, can serve as an effective natural attenuator of ambient vibrations, as demonstrated by Koley et al. (2019, 2022) and Bader et al. (2022). This consideration suggests that the northwestern part of the study area is particularly favorable, due to both its lower levels of surface disturbance and the presence of suitable geological cover. In contrast, the direct border region with Germany, especially near Aachen, is considered less suitable due to its high density of wind turbines and transportation infrastructure, which may introduce persistent environmental noise.

The geology of the study area is characterized by considerable complexity, comprising sedimentary formations of varying age and diagenetic origin. The location, wedged between the Variscan thrust front and the Lower Rhine Graben, resulted in a strong structural overprint and the development of locally complex discontinuity networks, particularly in proximity to fault zones. These discontinuities require careful consideration in the planning of cavern structures, as they pose a risk for structurally controlled instabilities such as block and wedge failures. They also influence subsurface groundwater flow, potentially affecting tunnel and cavern inflow conditions. Among the investigated units, the Upper Devonian sandstone–siltstone sequences of the Condroz Sandstone Group exhibit favorable geotechnical properties, including high compressive and tensile strengths, and thicknesses exceeding 100 m. These characteristics suggest good mechanical stability and suitability for efficient excavation, particularly in areas where the sequences are laterally homogeneous and unaffected by faulting. With appropriate

assessment of site-specific structural and hydrogeological conditions, these units present a promising candidate for hosting large cavern structures. The subsurface stress conditions require further assessment to define present stress orientations and magnitudes for safe infrastructure planning. However, stress-induced deformation and resulting instabilities (e.g., squeezing ground conditions) are conceivable in the soft rocks and sediments of the Upper Namurian and overlying Cretaceous formations. This is particularly relevant for the planning and construction of shafts, helical ramps, or tunnels that will provide access to the facilities, as they penetrate these soft cover layers. Borehole Ban-1 has demonstrated that soft rock layers may occur even at the planned final depth (250 m). Hydrogeological conditions may lead to significant water inflows into tunnels and chambers, necessitating special attention to appropriate dewatering measures and drainage systems.

The findings emphasize the importance of detailed site characterization, especially when selecting suitable cavern locations. Proximity to fault zones should be minimized to avoid structurally disturbed zones with poor rock mass quality. Where construction near faulted regions is unavoidable, robust support measures, particularly those designed to stabilize structurally defined wedges and blocks, must be incorporated into the excavation and design strategy. Tunnels will traverse a complex and variable geological succession. Fault zones, karst areas, and coal seams are likely to be encountered, each presenting specific challenges and demands to excavation and tunnel support. A seismic survey carried out under the E-TEST project covers parts of the study area, and will further support these efforts by (a) characterizing the contact depth between the Cretaceous and Paleozoic units and (b) mapping the spatial distribution of fault zones across the study area.

Collectively, the geological setting of the EMR offers promising characteristics for the Einstein Telescope, particularly due to the natural noise attenuation of soft geological units. At the same time, the subsurface conditions pose considerable challenges for underground construction, primarily due to their complex tectonic history, which introduces significant uncertainty in the continuity of lithological units and fault zones. Nevertheless, undisturbed zones, particularly within the Upper Devonian Condroz Sandstone Group, demonstrate favorable geotechnical characteristics, offering potential for stable mechanical tunnel and cavern excavation. This potential has already been demonstrated in the Soumagne train tunnel, located at the rim of the study area, where complex geological conditions were successfully managed through tailored appropriate tunneling approaches, detailed site investigations, and continuous monitoring.

Lastly, the authors emphasize that this study represents a preliminary feasibility assessment and does not replace the need for comprehensive site investigations. Intensive exploration efforts, including several boreholes and geophysical surveys, are currently underway to determine the most suitable positioning of the Einstein Telescope within the EMR, taking into account both the ambient noise field and construction feasibility. The ET layout proposed in this study should therefore be considered a conceptual starting point for discussion and planning, rather than a definitive design for the final implementation.

Acknowledgements The E-TEST project is carried out under the Interreg V-A Euregio Meuse-Rhine Programme, with €8.1 million from the European Regional Development Fund (ERDF). By investing EU funds in Interreg projects, the European Union directly invests in economic development, innovation, territorial development, social inclusion, and education in the Euregio-Meuse-Rhine. We thank the editor and reviewers for their constructive feedback and thorough review, which significantly helped to improve the quality and clarity of this study.

Funding Open Access funding enabled and organized by Projekt DEAL.

Declarations

Competing interests The authors declare that they have no conflict of interest.

References

Ahlers S, Henk A, Hergert T et al (2021a) The recent stress state of Germany – results of a geomechanical–numerical 3D model. Safety of Nuclear Waste Disposal 1:163–164. https://doi.org/10.5194/sand-1-163-2021

Ahlers S, Henk A, Hergert T et al (2021b) 3D crustal stress state of Germany according to a data-calibrated geomechanical model. Solid Earth 12:1777–1799. https://doi.org/10.5194/se-12-1777-2021

Akutsu T, Ando M, Araki S et al (2018) Construction of KAGRA: an underground gravitational-wave observatory. Prog Theor Exp Phys. https://doi.org/10.1093/ptep/ptx180.

Amann F, Bonsignorio F, Bulik T et al (2020) Site-selection criteria for the Einstein telescope. Rev Sci Instrum 91:094504. https://doi.org/10.1063/5.0018414

Amann F, Badaracco F, DeSalvo R et al (2022) Tunnel configurations and seismic isolation optimization in underground gravitational

wave detectors. Appl Sci 12:8827. https://doi.org/10.3390/app12178827
Bader M, Koley S, Van Den Brand J et al (2022) Newtonian-noise characterization at Terziet in Limburg—the euregio Meuse–Rhine candidate site for Einstein telescope. Classical Quantum Gravity 39:025009. https://doi.org/10.1088/1361-6382/ac1be4
Beker MG, van den Brand JFJ, Rabeling DS (2015) Subterranean ground motion studies for the Einstein telescope. Classical Quantum Gravity 32:025002. https://doi.org/10.1088/0264-9381/32/2/025002
Bevandić S, Blannin R, Vander Auwera J et al (2020) Geochemical and mineralogical characterisation of historic Zn–Pb mine waste, Plombières, East Belgium. Minerals 11:28. https://doi.org/10.3390/min11010028
Bieniawski ZT (1989) Engineering rock mass classifications: a complete manual for engineers and geologists in mining, civil, and petroleum engineering. Wiley, New York
Bless MJM, Bouckaert J, Conil R et al (1980) Pre-permian depositional environments around the Brabant Massif in Belgium, the Netherlands and Germany. Sediment Geol 27:1–81. https://doi.org/10.1016/0037-0738(80)90031-7
Bless MJM, Bouckaert J, Paproth E (1983) Recent exploration in Pre-Permian rocks around the Brabant Massif in Belgium, the Netherlands and the federal Republic of Germany. In: Kaasschieter JPH, Reijers TJA (eds) Petroleum geology of the southeastern North sea and the adjacent onshore areas. Springer Netherlands, Dordrecht, p pp 51-62
Bless MJM, Felder PJ, Meessen PMT (1986) Late cretaceous sea level rise and inversion: their influence on the depositional environment between Aachen and Antwerp. Ann De La Société géologique Belgique 109:333–355
Boese CM, Wotherspoon L, Alvarez M, Malin P (2015) Analysis of anthropogenic and natural noise from multilevel borehole seismometers in an urban environment, Auckland, New Zealand. Bull Seismol Soc Am 105:285–299. https://doi.org/10.1785/0120130288
Branchesi M, Maggiore M, Alonso D et al (2023) Science with the Einstein telescope: a comparison of different designs. J Cosmol Astropart Phys 2023:068. https://doi.org/10.1088/1475-7516/2023/07/068
Brenguier F, Boué P, Ben-Zion Y et al (2019) Train traffic as a powerful noise source for monitoring active faults with seismic interferometry. Geophys Res Lett 46:9529–9536. https://doi.org/10.1029/2019GL083438
Brisson S, Wellmann F, Chudalla N et al (2023) Estimating uncertainties in 3-D models of complex fold-and-thrust belts: a case study of the Eastern Alps triangle zone. Appl Comput Geosci 18:100115. https://doi.org/10.1016/j.acags.2023.100115
Cambier G, Dejonghe L (2010) Systematic inventory and ordering of faults in Belgium - Part 1. Geological Survey of Belgium
Cambier G, Dejonghe L (2012) Systematic inventory and ordering of faults in Belgium - Part 2. Geological Survey of Belgium
Camelbeeck T, Vanneste K, Alexandre P et al (2007) Relevance of active faulting and seismicity studies to assessments of long-term earthquake activity and maximum magnitude in intraplate Northwest Europe, between the lower rhine embayment and the North sea. In: Stein S, Mazzotti S (eds) Special Paper 425: Continental intraplate earthquakes: Science, Hazard, and policy issues. Geological Society of America, pp 193-224. https://doi.org/10.1130/2007.2425(14)
Cheng W-C, Cui Q-L, Shen J et al (2017) Fractal prediction of grouting volume for treating karst caverns along a shield tunneling alignment. Appl Sci 7:652. https://doi.org/10.3390/app7070652
De La Varga M, Schaaf A, Wellmann F (2019) GemPy 1.0: open-source stochastic geological modeling and inversion. Geosci Model Dev 12:1–32. https://doi.org/10.5194/gmd-12-1-2019
Deckers J, Rombaut B, Broothaers M et al (2023) New 3d fault model for Eastern Flanders (Belgium) providing insights on the major deformation phases in the region since the late paleozoic. J Struct Geol 166:104779. https://doi.org/10.1016/j.jsg.2022.104779
Dejonghe L (1998) Zinc–lead deposits of Belgium. Ore Geol Rev 12:329–354. https://doi.org/10.1016/S0169-1368(98)00007-9
Di Pace S, Mangano V, Pierini L et al (2022) Research facilities for Europe's next generation gravitational-wave detector Einstein telescope. Galaxies 10:65. https://doi.org/10.3390/galaxies10030065
ET Steering Committee Editorial Team (2020) Design Report Update 2020 for the Einstein Telescope. https://apps.et-gw.eu/tds/?r=18715
ET Science Team (2011) Einstein gravitational wave Telescope conceptual design study
European Union (2019) Managing natura 2000 sites: the provisions of Article 6 of the 'Habitats' Directive 92/43/EEC. https://data.europa.eu/doi/10.2779/02245
Evrard M, Dumont G, Hermans T et al (2018) Geophysical investigation of the Pb–Zn deposit of Lontzen–Poppelsberg, Belgium. Minerals 8:233. https://doi.org/10.3390/min8060233
Farhadian H, Nikvar-Hassani A (2019) Water flow into tunnels in discontinuous rock: a short critical review of the analytical solution of the art. Bull Eng Geol Environ 78:3833–3849. https://doi.org/10.1007/s10064-018-1348-9
Fiori I, Effler A, Nguyen P et al (2021) Environmental noise in Gravitational-Wave interferometers. In: Bambi C, Katsanevas S, Kokkotas KD (eds) Handbook of gravitational wave astronomy. Springer Singapore, Singapore, pp 1–72
Freise A, Chelkowski S, Hild S et al (2009) Triple Michelson interferometer for a third-generation gravitational wave detector. Classical Quantum Gravity 26:085012. https://doi.org/10.1088/0264-9381/26/8/085012
Freise A, Hild S, Somiya K et al (2011) Optical detector topology for third-generation gravitational wave observatories. Gen Relativ Gravit 43:537–567. https://doi.org/10.1007/s10714-010-1018-0
Geluk MC, Duin EJTh, Dusar M et al (1994) Stratigraphy and tectonics of the Roer Valley Graben. Geologie en Mijnbouw 73:129–141
Goel RK (2016) Experiences and lessons from the use of TBM in the Himalaya – a review. Tunn Undergr Space Technol 57:277–283. https://doi.org/10.1016/j.tust.2016.02.015
Gong Q, Liu Q, Zhang Q (2016) Tunnel boring machines (TBMs) in difficult grounds. Tunn Undergr Space Technol 57:1–3. https://doi.org/10.1016/j.tust.2016.05.010
Haimson BC, Cornet FH (2003) ISRM suggested methods for rock stress estimation—Part 3: hydraulic fracturing (HF) and/or hydraulic testing of pre-existing fractures (HTPF). Int J Rock Mech Min Sci 40:1011–1020. https://doi.org/10.1016/j.ijrmms.2003.08.002
Hance L, Dejonghe L, Ghysel P et al (1999) Influence of heterogeneous lithostructural layering on orogenic deformation in the variscan front zone (eastern Belgium). Tectonophysics 309:161–177. https://doi.org/10.1016/S0040-1951(99)00137-7
Heidbach O, Rajabi M, Cui X et al (2018) The world stress map database release 2016: crustal stress pattern across scales. Tectonophysics 744:484–498. https://doi.org/10.1016/j.tecto.2018.07.007
Hemphill GB (2012) Practical tunnel construction, 1st edn. Wiley
Hild S, Abernathy M, Acernese F et al (2011) Sensitivity studies for third-generation gravitational wave observatories. Classical Quantum Gravity 28:094013. https://doi.org/10.1088/0264-9381/28/9/094013
Hoek E (1994) Strength of rock and rock masses. ISRM News J 2:4–16
Hoek E, Carranza-Torres C, Corkum B (2002) Hoek-Brown failure criterion - 2002 Edition. In: Proc. NARMS-TAC Conference, Toronto, 1:267–273

Hoek E (2007) Practical-Rock-Engineering. RocScience. https://www.rocscience.com/learning/hoeks-corner

Hollmann EG (1997) Der variszische Vorlandüberschiebungsgürtel der Ostbelgischen Ardennen: ein bilanziertes Modell, 1. Aufl. Verl. der Augustinus Buchh, Aachen

Houtgast RF, van Balen RT (2000) Neotectonics of the Roer Valley rift system, the Netherlands. Glob Planet Change 27:131–146. https://doi.org/10.1016/S0921-8181(01)00063-7

Janssens B, Bouhenni S, Dethy B et al (2005) Le tunnel TGV de Soumagne (Belgique) et ses difficultés géologiques. Géoline Lyon 23–25

Jeong H, Choi S, Lee Y-K (2023) Evaluation of cutting performance of a TBM disc cutter and cerchar abrasivity index based on the brittleness and properties of rock. Appl Sci 13:2612. https://doi.org/10.3390/app13042612

Käsling H, Plinninger RJ (2022) Empfehlung Nr. 23: bestimmung der Abrasivität von gesteinen Mit dem CERCHAR-Versuch. In: Deutschen Gesellschaft für Geotechnik e. V. (DGGT) (ed) Empfehlungen des arbeitskreises versuchstechnik fels, 1st edn. Wiley, pp 329–339

Koley S, Bader M, Bertolini A et al (2019) Seismic characterization of the euregio Meuse-Rhine in view of Einstein Telescope - First results of seismic studies of the Belgian-Dutch-German site for Einstein Telescope 14. https://www.nikhef.nl/wp-content/uploads/2019/10/Terziet-Drilling-Campaign-Final-NoC.pdf

Koley S, Bader M, van den Brand J et al (2022) Surface and underground seismic characterization at Terziet in Limburg—the euregio Meuse–Rhine candidate site for Einstein telescope. Classical Quantum Gravity 39:025008. https://doi.org/10.1088/1361-6382/ac2b08

Laloux M, Geukens F, Ghysel P et al (2000) Geological map of Wallonia. Gemmenich -Botzelaar. Henri-Chapelle-Raeren, Petergensfeld-Lammersdorf

LaMoreaux JW (2019) Environmental geology. Springer US, New York, NY

Lepique M (2022) Empfehlung Nr. 10: indirekter Zugversuch an Gesteinsproben – Spaltzugversuch. In: Deutschen Gesellschaft für Geotechnik e. V. (DGGT) (ed) Empfehlungen des arbeitskreises versuchstechnik fels, 1st edn. Wiley, pp 115–122.

Li J, Chen Q, Huang X et al (2021) Pretreatment for tunnel karst cave during excavation: a case study of Guangxi, China. Adv Civil Eng 2021:1–12. https://doi.org/10.1155/2021/9013815

Limberger F, Rümpker G, Lindenfeld M, Deckert H (2023) The impact of seismic noise produced by wind turbines on seismic borehole measurements. Solid Earth 14:859–869. https://doi.org/10.5194/se-14-859-2023

Marinos P, Hoek E (2000) GSI: A Geologically Friendly Tool for Rock Mass Strenght Estimation. In: GeoEng 2000 at the International Conference on Geotechnical and Geological Engineering, Melbourne, 19–24 November 2000,. Melbourne, pp 1422–1446

Masset O, Loew S (2010) Hydraulic conductivity distribution in crystalline rocks, derived from inflows to tunnels and galleries in the central Alps, Switzerland. Hydrogeol J 18:863–891. https://doi.org/10.1007/s10040-009-0569-1

Mönnig C (2007) Urban land use detection and change using an enhanced monitoring system with remote sensing tools and GIS in the EUREGIO Meuse-Rhine area. Aachen Techn Hochsch Diss

Morawietz S, Heidbach O, Reiter K et al (2020) An open-access stress magnitude database for Germany and adjacent regions. Geotherm Energy 8:25. https://doi.org/10.1186/s40517-020-00178-5

Mottequin B, Denayer J, Delcambre B et al (2024) Upper devonian lithostratigraphy of Belgium. Geol Belg 27:193–270. https://doi.org/10.20341/gb.2024.010

Müller B, Zoback ML, Fuchs K et al (1992) Regional patterns of tectonic stress in Europe. J Geophys Res 97(B8):11783–11803. https://doi.org/10.1029/91JB01096

Mutschler T (2022) Empfehlung Nr. 1: einaxiale Druckversuche an Zylindrischen Gesteinsprüfkörpern. In: Deutschen Gesellschaft für Geotechnik e. V. (DGGT) (ed) Empfehlungen des arbeitskreises versuchstechnik fels, 1st edn. Wiley, pp 1–20

Neuffer T, Kremers S (2017) How wind turbines affect the performance of seismic monitoring stations and networks. Geophys J Int 211:1319–1327. https://doi.org/10.1093/gji/ggx370

ÖGG (2021) Richtlinie für die geotechnische Planung von Untertagebauten mit zyklischem Vortrieb, 3rd edn. Austrian Society for Geomechanics

Poty E (2016) The Dinantian (Mississippian) succession of Southern Belgium and surrounding areas: stratigraphy improvement and inferred climate reconstruction. Geol Belg 19:177–200. https://doi.org/10.20341/gb.2016.014

Poty E, Delculée S (2011) Interaction between eustacy and block-faulting in the carboniferous of the Visé - Maastricht area (Belgium, the Netherlands). Zdgg 162:117–126. https://doi.org/10.1127/1860-1804/2011/0162-0117

Punturo M, Abernathy M, Acernese F et al (2010) The Einstein telescope: a third-generation gravitational wave observatory. Classical Quantum Gravity 27:194002. https://doi.org/10.1088/0264-9381/27/19/194002

Reiter K, Heidbach O, Müller B et al (2016) Stress Map Germany. https://doi.org/10.5880/WSM.Germany2016

Ronchini S, Branchesi M, Oganesyan G et al (2022) Perspectives for multimessenger astronomy with the next generation of gravitational-wave detectors and high-energy satellites. A&A 665:A97. https://doi.org/10.1051/0004-6361/202243705

Saccorotti G, Piccinini D, Cauchie L, Fiori I (2011) Seismic noise by wind farms: a case study from the Virgo gravitational wave Observatory, Italy. Bull Seismol Soc Am 101:568–578. https://doi.org/10.1785/0120100203

Sathyaprakash B, Abernathy M, Acernese F et al (2012) Scientific objectives of Einstein telescope. Classical Quantum Gravity 29:124013. https://doi.org/10.1088/0264-9381/29/12/124013

Singh B, Goel RK (2011) Support system in caverns. In: Singh B, Goel RK (eds) Engineering rock mass classification. Elsevier, pp 159–167. https://doi.org/10.1016/B978-0-12-385878-8.00033-1

Solak T (2009) Ground behavior evaluation for tunnels in blocky rock masses. Tunnelling Underground Space Technol 24:323–330. https://doi.org/10.1016/j.tust.2008.10.004

Somiya K (2012) Detector configuration of KAGRA–the Japanese cryogenic gravitational-wave detector. Classical Quantum Gravity 29:124007. https://doi.org/10.1088/0264-9381/29/12/124007

Tacim G, Posluk E, Gokceoglu C (2023) Importance of grouting for tunneling in karstic and complex environment (a case study from Türkiye). Geo-Engineering 14:6. https://doi.org/10.1186/s40703-023-00183-0

Teymen A (2020) The usability of cerchar abrasivity index for the estimation of mechanical rock properties. Int J Rock Mech Min Sci 128:104258. https://doi.org/10.1016/j.ijrmms.2020.104258

Thorez J, Dreesen R, Streel M (2006) Famennian. In: Dejonghe, L., ed., Current status of chronostratigraphic units named from Belgium and adjacent areas. Brussels, pp 27–45

Thuro K (2010) Empfehlung Nr. 5 Punktlastversuche an Gesteinsproben des arbeitskreises 3.3 versuchstechnik fels der Deutschen gesellschaft für geotechnik. Bautechnik 87:322–330. https://doi.org/10.1002/bate.201010025

TNO (2004) Geological atlas of the subsurface of the Netherlands - onshore. Netherlands Institute of Applied Geoscience TNO - National Geological Survey, Utrecht

Torabi A, Berg SS (2011) Scaling of fault attributes: a review. Mar Pet Geol 28:1444–1460. https://doi.org/10.1016/j.marpetgeo.2011.04.003

Torabi A, Johannessen MU, Ellingsen TSS (2019) Fault core thickness: insights from siliciclastic and carbonate rocks. Geofluids 2019:1–24. https://doi.org/10.1155/2019/2918673

Trautwein-Bruns U, Schulze KC, Becker S et al (2010) In situ stress variations at the variscan deformation front — results from the deep Aachen geothermal well. Tectonophysics 493:196–211. https://doi.org/10.1016/j.tecto.2010.08.003

Trautwein-Bruns U, Hilgers C, Becker S et al (2011) Bruch- und Störungssysteme in der Übergangszone Zwischen der Niederrheinischen Bucht und dem Rheinischen schiefergebirge Im belgisch-deutschen Grenzbereich - Ergebnisse der bohrung RWTH-1. Aachen Deutschland Zdgg 162:251–275. https://doi.org/10.1127/1860-1804/2011/0162-0251

von Winterfeld C-H (1994) Variszische Deckentektonik und devonische Beckengeometrie der Nordeifel: ein quantitatives Modell; (Profilbilanzierung und Strain-Analyse im Linksrheinischen Schiefergebirge), 1. Aufl. Verl. der Augustinus-Buchh, Aachen

Walter R (2007) Geologie von mitteleuropa, 7th edn. E. Schweizerbart'sche Verlagsbuchhandlung, Stuttgart

Walter R (2010) Aachen und südliche umgebung: Nordeifel und Nordost-Ardennen. Gebr. Borntraeger, Berlin

Wellmann JF, Horowitz FG, Schill E, Regenauer-Lieb K (2010) Towards incorporating uncertainty of structural data in 3D geological inversion. Tectonophysics 490:141–151. https://doi.org/10.1016/j.tecto.2010.04.022

Zieger T (2019) Experimental quantification of seismic signals induced by wind turbines. Karlsruher Institut für Technologie (KIT) https://doi.org/10.5445/IR/1000096453

Zieger T, Ritter JRR (2018) Influence of wind turbines on seismic stations in the upper rhine graben, SW Germany. J Seismol 22:105–122. https://doi.org/10.1007/s10950-017-9694-9